# Structural analysis of the middle domain of the poly(A)-binding protein-interacting protein 1 (MPaip1)

Ahmad Seif Kanaan January, 2010



A thesis submitted to McGill University in partial fulfillment of the requirements of the degree of Master of Science under the Faculty of Medicine

© AHMAD SEIF KANAAN, 2009
Groupe de Recherche Axé sur la Structure des proteins (GRASP)
Department of Biochemistry
McGill University
Montreal, QC

#### **ACKNOWLEDGEMENTS**

Many individuals have been instrumental in the course of this study. My first and most enduring acknowledgement is to Dr. Bhushan Nagar. I am grateful for his mentorship and guidance throughout my training, for his encouragement in times of scientific despair and for his keen scientific eye. Special thanks are also in order to the highly skilled German Scientist Filipp Frank. His mentorship, assistance and motivation shall never be forgotten. I warmly thank Yazan Abbas for his guidance at the outset of my training, for his undiminished troubleshooting assistance and for his true and enduring friendship. I am also grateful to Lama Talje for first introducing me to the methods of protein purification and crystallization. I thank all past and present members of the Nagar lab: Rose Szittner, Geneviève Virgili, Alexei Gorelik, Katalin Illes, Karan Verma and Cheslea Maedler-Kron for any assistance they may have imparted and for creating a pleasant scientific atmosphere. I thank Dr. Sonenberg for his collaboration; my research advisory committee members: Drs. Kalle Gehring and Jason Young for their helpful comments and recommendations; Dr. Jean-François Trempe and Dr. Guennadi Kozlov for assistance in data collection at the CHESS synchrotron; Dr. Richard Marcellus for his aid in Surface Plasmon Resonance, Dr. Yvan Martineau for countless helpful discussions; Dr. Alan Matte for assistance in SeMet diffraction testing at the NRC-BRI; the GRASP committee for granting me a travel award for the American Crystallographic Association conference where these results were presented; all members of the Berghuis, Gehring and Young laboratories for their selflessness in equipment and instrument use; Tareg and Mona Kanaan for being there when it counted; and Dr. Kirsten Müller for pointing out the door of science and discovery.

This work would not have been possible without the vision of the major catalyst Seif Kanaan; the love and inspiration of the mitochondrial powerhouse Shireen Kanaan; the affection and adoration of the resilient Farah Kanaan; and the natural effervescence of Mira Kanaan.

# **CONTENTS**

ACK	NOWL	_EDGEMENTS	2
LIST	OF T	ABLES & FIGURES	5
ABB	REVIA	ATIONS	6
ABS	TRAC	Т	8
1.	INTRO	DDUCTION	10
1.	1. Ge	ene regulation	10
1.	2. Tra	anslation initiation	10
1.	3. Eu	karyotic translation initiation factors (eIFs) direct cap-dependent initiation	12
1.	4. Th	e closed loop model of mRNA translation	15
1.	5. PA	ABP-Interacting Proteins 1 and 2 (Paips)	18
1.	6. Pa	ip1	19
1.	7. Pa	ip1 implicated in mRNA turnover	21
		thological relevance of Paip1 in familial Amyotrophic lateral sclerosis (FAI	
1.	9. Re	gulation of Paip Proteins	23
1.	10.	Structure of MIF4G homologs	25
1.	11. /	Aims of the study	26
2.	MATE	RIALS AND METHODS	27
2.	1. MA	ATERIALS	27
	2.1.1.	Chemicals	27
	2.1.2.	Buffers, solutions and Kits	28
	2.1.3.	Cell growth media	29
2.	2. ME	ETHODS	30
	2.2.1.	General Procedures	30
	2.2.2.	Paip1 and eIF4A Plasmid preparation	32
	2.2.3. 371) a	Protein expression of Paip1 plasmids; Paip1, Paip1 (157-371), Paip1 (19nd Paip1 (154-479)	
	2.2.4.	Protein expression of Se-Met Paip1(157-371)	33
	2.2.5.	Protein expression of recombinant eIF4A	34
	2.2.6.	Protein Purification	35
	2.2.6.1	Immobilized metal affinity chromatography (IMAC)	35
	2.2.6.2	2. Anion Exchange chromatography (AEC)	35
	2.2.6.3	3. Size-exclusion chromatography (SEC)	36

	2.2	.7.	Crystallization	36		
	2.2	.8.	X-ray diffraction and Data collection	37		
	2.2	.9.	Phasing, Model building and Refinement	37		
	2.2	.10.	Small Angle X-ray Scattering (SAXS)	37		
	2.2	.11.	Pull down experiments	38		
	2.2	.12.	Isothermal Titration Calorimetry (ITC)	39		
	2.2	.13.	Surface Plasmon Resonance (SPR)	39		
3.	RE	SUL	TS AND DISCUSSION	40		
,	3.1.	Clo	ning and Expression	40		
,	3.2.	Pur	ification of Paip1 constructs and eIF4A	41		
,	3.3.	Cry	stallization of MPaip1	45		
,	3.4.	Diff	raction screening and molecular replacement	47		
,	3.5.	Exp	ression, Purification and Mass spectrometry of SeMet MPaip1	49		
,	3.6.	Diff	raction, phasing and data analysis	51		
,	3.7.	MP	aip1 Structural overview	52		
,	3.8.	Stru	uctural and functional comparisons of MPaip1 and MIF4G	57		
,	3.9.	Bin	ding studies	63		
,	3.10.	S	mall angle X-ray Scattering (SAXS) analysis of MPaip1	65		
4.	CO	NCL	USION	69		
RF	REFERENCES 7					

## **LIST OF TABLES & FIGURES**

Figure 1 Simplified schematic model of eukaryotic translation initiation (Kuersten and Goodwin, 2003)
Figure 2 Translation initiation factors and the regulation of initiation (Sonenberg and
Hinnebusch, 2009).
Figure 3 The closed loop model of mRNA (Svitkin and Sonenberg, 2006)1
Figure 4 Structural organization and interactions of PABP and Paips (Derry et al., 2006)
1i
Figure 5 Structural organization of motifs common between Paip1 and eIF4G119
Figure 6 Model of Paip1 enhancement of Translation20
Figure 7 Crystal structure of the yeast eIF4A-eIF4G complex highlighting the key Tr
residue (W579) (Schutz et al., 2008)2
Figure 8 PROF Prediction of the secondary structure of Paip1 (143-479) 40
Figure 9 Chromatogram and SDS-PAGE (inset) of the Ni affinity purification step of
MPaip1
Figure 10 Chromatogram and SDS-PAGE(inset) of the anion exchange purification ste
of MPaip1
Figure 11 Chromatogram of analytical gel filtration and SDS-PAGE analysis (inset) of
purified MPaip144 Figure 12 Initial screening and optimization crystals of MPaip14
Figure 13 Representative X-ray diffraction patterns of MPaip1 obtained on a home rotating-anode source
Figure 14 Harker section (v=0.5) from the native Patterson function of MPaip1 diffraction
data4
Figure 15 Mass spectrometry analysis of native MPaip1 SeMet MPaip150
Table 1 Crystal parameters and data-collection statistics for MPaip1 crystals 5
Figure 16 X-ray Crystal Structure of MPaip1 (Paip1 <sub>157-375</sub> )
Figure 17 Multiple Sequence Alignment of several MPaip1 orthologs and homologs 5
Figure 18 Surface representation of MPaip1 residues conserved among all know
species50
Figure 19 Electrostatic surface rendition of MPAIP150
Figure 20 Overlay of MPaip1 on human and yeast MIF4G5
Figure 21 Crystal structures of MPaip1, MIF4GI and MIF4GII60
Figure 22 Surface representation of eIF4A conserved binding sites on MPAIP16
Table 2 List of the eIF4A binding sites of yeast MIF4GI (TIF4631) generated by the
PROTROP server and their conservation indices with MPaip1
Figure 23 SDS-PAGE analysis of Paip1, MPaip1 and eIF4A pull-down experiments 6
Figure 24 SAXS results for MPaip1
Figure 25 Three views of the MPaip1 SAXS model reconstructed ab initio using
GASBOR (Svergun et al., 2001) 68

#### **ABBREVIATIONS**

1HU3 PDB ID for human MIF4G

2VSO PDB ID for yeast MIF4G in complex with eIF4A

5p Short arm of chromosome of 5

A site Aminoacyl site of the 40S ribosome AEC Anion exchance chromatography

Amp Ampicillin

c-fos mRNA Cellular proto-oncogene

CHESS Cornell high energy synchrotron source

CNI Copy number increase

CRD Protein-coding region determinants of instability

DAP-5 Death associated protein 5 (p97)

Dmax Maximum dimension of scattering particle

dsDNA Double stranded DNA

DTT Dithiothreitol

EDD Human orthologue of the hyperplastic discs protein

eIF3 Eukaryotic initiation factor 3
eIF4A Eukaryotic initiation factor 4A
eIF4E Eukaryotic initiation factor E
eIF4F Eukaryotic initiation factor F
eIF4G Eukaryotic initiation factor G
eIF5 Eukaryotic initiation factor 5
eIFs Eukaryotic initiation factors

FALS Familial amyotrophic lateral sclerosis FISH Fluorescence in situ hybridization

FL Full length

FPLC Fast protein liquid chromatography

GDP Guanosine diphosphate
GTP Guanosine triphosphate

IMAC Immobilized metal affinity chromatography IPTG Isopropyl β-D-1-thiogalactopyranoside

ITC Isothermic titration calirometry

LB Luria Bertani Medium
M9 Minimal growth medium

MAD Multiwavelength anomalous dispersion

mCRD Major coding region determinants of instability

MIF4G Middle domain of elf4G MPAIP1 Middle domain of Paip1

mRNA Messenger RNA

mTOR Mammalian target of rapamycin

P site Peptidyl decoding site of the 40S ribosome

PABP Poly(A)-Binding protein

Paip1 Poly(A)-binding protein Interacting Protein 1
Paip2 Poly(A)-binding protein Interacting Protein 2

PAM PABP binding motif PEG Poly(ethylene glycol)

PROF Profile network prediction Heidelberg
Protorp Protein-Protein interface analysis server

Rg Radius of Gyration

RMSD Root mean square deviation

RNP Ribonucleoprotein RNA recognition motif

SAD Single wavelength anomalous dispersion

SAXS Small angle X-ray scattering

SDS-PAGE Sodium dodecyl sulfate polyacrylamide gel

electrophoresis

SEC Size exculsion chromatography

SeMet Selenomethionine siRNA Small interfering RNA

SNP Single nucleotide polymorphism

SOC Super Optimal Broth
SOD1 Superoxide dismutase 1
SPR Surface Plasmon resonance
TBE Tris/Borate/EDTA Buffer

TCEP Tris(2-carboxyethyl)phosphine

TEV Tobacco Etch virus
TgM Transgenic mice

UTR 5' untranslated region of mRNA

ZYM-5052 Auto-Inducing medium of the Studier Method

#### **ABSTRACT**

Initiation is the rate-limiting step in the process of translation, which is a complex process that requires the participation of numerous translation initiation factors (eIFs). The poly (A)-binding protein (PABP) interacts simultaneously with the poly(A) tail of mRNAs and the scaffolding protein elF4G to mediate mRNA circularization resulting in the stimulation of protein translation. PABP is regulated by the PABP-interacting protein, Paip1. Paip1 is thought to act as a translational activator in 5' cap dependent translation by interacting with PABP and the initiation factors eIF4A and eIF3. In this study, the Xray crystal structure of the middle domain of Paip1 (MPaip1; spanning 157-371) has been determined to a 1.7 Å resolution, revealing a crescent-shaped domain consisting of ten alpha helices arranged as five  $\alpha$ -HEAT repeats. I show that the interaction of fulllength Paip1 with eIF4A is very weak, suggesting that it is merely a stabilizing interaction in the translation initiation complex. Binding analysis between MPaip1 and elF4A utilizing pull-down experiments, isothermal titration calorimetry and surface plasmon resonance, show that unlike MIF4G (the middle of domain of eIF4G), MPaip1 does not bind eIF4A. This suggests that the weak interaction between Paip1 and eIF4A is mediated by residues upstream or downstream of the middle domain.

## **RÉSUMÉ**

L'initiation est l'étape déterminante de vitesse de réaction dans la traduction, un processus complexe qui requiert la participation d'un grand nombre de facteurs d'initiation. PABP (la protéine qui se lie à la queue poly(A) de l'ARNm) interagit simultanément avec l'ARNm et la protéine d'échaffaudage elF4G, ce qui déclenche la circularization de l'ARNm et stimule la synthèse de protéines. PABP est régulée par la protéine Paip1. Paip1 est suggérée être activatrice du processus de traduction medié par la coiffe 5' de l'ARNm, par son interaction avec PABP et les facteurs d'initiation elF4A et elF3. Dans cette étude, la structure du domaine du milieu de Paip1 (Mpaip1, comprenant 157-371) a été résolué à travers la cristallographie par rayons X, à une résolution de 1.7 Å. Cette structure a révélé un domaine en forme de croissant, contenant 10 hélices alpha formant cinq HEAT repeats. Je montre que l'interaction du domaine complet de Paip1 avec elF4A est très faible, suggérant qu'elle constitute simplement une interaction stabilizante dans le complexe d'initiation de traduction. Une analyse de l'interaction entre Mpaip1 et eIF4A en utilisant des expériences de pulldown, ITC et SPR, montre qu'au contraire de MIF4G (le domaine du milieu de elF4G), Mpaip1 ne se lie pas à eIF4A. Cela suggère que l'interaction faible entre Paip1 et eIF4A est médiée par des résidues en montée ou en aval du domain du milieu.

#### 1. INTRODUCTION

#### 1.1. Gene regulation

The regulation of gene expression is a process fundamental to the vitality of an organism. Gene expression can be regulated at multiple levels which include transcription, RNA splicing, transport and translation, in addition to protein activity by post translational modification. Multilevel gene regulation gives the cell more control over its structure and function and, thus, its differentiation, morphogenesis, versatility and adaptability (Sonenberg and Hinnebusch, 2009). While most genes are regulated at the level of transcription, regulation at the final level of the flow of genetic information is more direct and more rapid at balancing cellular concentrations of encoded proteins (Holcik and Sonenberg, 2005). This fact is due to the time lag associated with mRNA synthesis, processing and export (Holcik and Sonenberg, 2005). Moreover, the lack of correlation between mRNA and protein levels in numerous genes indicates that translational control carries a greater regulatory weight (Holcik and Sonenberg, 2005). Eukaryotic translational control is critical for gene regulation during stress, nutrient deprivation, development, differentiation, nervous system function, aging and disease (Holcik and Sonenberg, 2005; Sonenberg and Hinnebusch, 2009). The process of translation is broadly divided into initiation, elongation, termination and ribosome recycling. Given that the first phase of translation is the rate limiting step, translational regulation predominantly occurs at the level of initiation, when the ribosome is recruited to the AUG start codon site on an mRNA (Sonenberg and Hinnebusch, 2009).

#### 1.2. Translation initiation

Translation initiation is a complex process that utilizes numerous initiation factors (eIFs). eIFs carry out a number of steps to place the AUG start codon in the peptidyl decoding (P) site of the ribosome following the scanning of mRNA in the 5'-3' direction (Figure 1). An initiator tRNAi, 40S, and 60S ribosomal subunits are assembled

by eukaryotic initiation factors into an 80S ribosome at the initiation codon. All eukaryotic mRNA molecules have a cap structure at the 5' end (m7GpppN, where m is a methyl group and N is any nucleotide) (Shatkin, 1976) and most have a poly(A) tail at the 3' end (Wickens, 1990). The 5' cap structure is important for mRNA stability which in turn affects the efficiency of protein synthesis (Shatkin, 1976). Uncapped mRNAs generally direct protein synthesis at lower efficiency than their capped counterparts in *in vitro* translation systems (Muthukrishnan et al., 1975). The poly(A) tail also plays an important role in determining both mRNA stability and translational efficiency (Jacobson and Peltz, 1996).

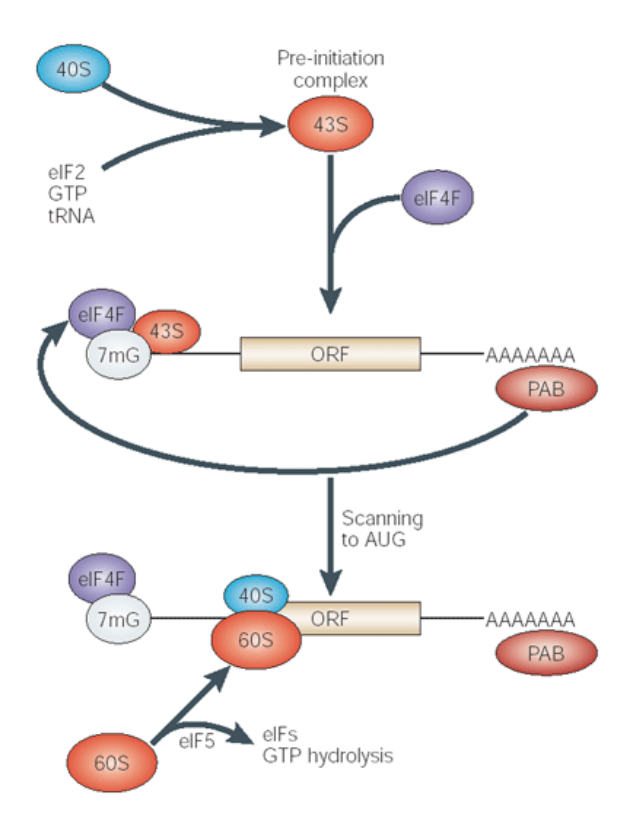


Figure 1 Simplified schematic model of eukaryotic translation initiation (Kuersten and Goodwin, 2003).

The figure illustrates a simplified view of translation initiation in eukaryotes showing several key factors. The 43S preinitiation complex (PIC) first forms with the association of the tRNAi, eIF2-GTP, eIF3, including other association factors to the 40S ribosomal subunit. The eIF4F complex is then able to recruit the 43S PIC to the 5' cap structure of the mRNA by interacting with ribosome associated factor eIF3. The poly(A) binding protein (PABP; designated PAB in this figure) which is associated with poly(A) tail at the 3' end, facilitates translation by communicating with cap bound eIF4F resulting in the circularization of mRNA. The PIC then scans downstream, and upon start codon recognition, eIF5 (not shown) hydrolyzes the GTP to join the 60S ribosomal subunit, thus generating an 80S ribosome that is translationally functional.

The process of translation may occur through a cap-dependant or a cap-independent mechanism. Cap-dependent translation occurs via the recruitment of a preassembled 43S pre-initiation complex (PIC) to the 5' cap end of the mRNA where the PIC scans downstream inspecting successive codons through its P-site till the AUG codon is reached (Merrick, 2004). PIC is composed of Met-tRNAi and eIFs 1,1A, 2,3 and 5. Complementarity to the anticodon of Met-tRNAi, which is anchored to PIC by eIF2-GTP, triggers the arrest of mRNA scanning by the irreversible hydrolysis of the GTP. At this point, eIF2-GDP is released allowing other eIFs to join the 60S subunit forming an 80S initiation complex. This signals the beginning of elongation where the initiation complex accepts the correct aminoacyl-tRNAi into the aminoacyl (A) site for the synthesis of peptides (Pestova and Hellen, 2000).

While the cap-dependant mechanism occurs in most cells, capindependent translation occurs in 3-5% of cellular mRNAs, enabling the synthesis of
specific proteins under the conditions in which cap-dependent translation is inhibited
(Blaszczyk et al., 2007; Johannes et al., 1999). Such proteins may play important roles
during the cell cycle, apoptosis, cancer development and stress responses (Blaszczyk
et al., 2007). Cap independent initiation utilizes internal ribosome entry sites (IRES),
which are located in the 5' untranslated region (UTR) of certain mRNAs, directing the
binding of the small ribosomal subunit by folding into a specific secondary and tertiary
structures (Merrick, 2004).

## 1.3. Eukaryotic translation initiation factors (eIFs) direct capdependent initiation

Cap-dependent initiation commences once the 5' cap structure is bound to eIF4F (Figure 2). eIF4F is a 250 kDa heterotrimeric complex, – consisting of eIF4E, eIF4A and eIF4G – that plays a pivotal role in initiation by bridging the mRNA and the

ribosome (Gingras et al., 1999a). eIF4E, a 25kDa protein, is a 5'-cap binding protein that is essential for efficient cap-dependent translation. It associates with the cap structure through its recruitment to the N-terminus of eIF4G. (Morino et al., 2000) eIF4E is the least abundant in the heterotrimeric complex, and as a result, it plays a critical regulatory role (Duncan et al., 1987). eIF4A, a 46kDa polypeptide, is a bidirectional ATP-dependent RNA helicase and an RNA-dependent ATPase (Lorsch and Herschlag, 1998; Ray et al., 1985; Rozen et al., 1990). It is responsible for unwinding secondary structures in the 5'-UTR of the mRNA with the aid of eIF4H and eIF4B (Rogers et al., 2001); thus creating a single stranded RNA segment to allow the binding of the 43S ribosomal subunit (Gingras et al., 1999b). eIF4A is recruited to the mRNA through eIF4G which has two distinct eIF4A binding sites (Imataka et al., 1997; Korneeva et al., 2001; Lamphear et al., 1995)(ref here). eIF4A belongs to the DEAD-box protein family, which partake in diverse processes apart from translation, including pre-mRNA splicing, ribosome biogenesis, and development (Linder and Slonimski, 1989).

eIF4G is a multi-scaffolding protein that serves to colocalize eIFs associated with the recruitment of the ribosome to the mRNA. eIF4G bridges eIF4A and eIF4E, and interacts with eIF3, the poly(A)- binding protein (PABP) and Mnk (a serine/threonine kinase that phosphorylates eIF4E, among other factors. eIF4G is a dynamic scaffold that adopts a number of conformational states in order to build the ribonucleorprotein complex necessary for initiation of translation (Prevot et al., 2003). There are two isoforms of eIF4G in mammals – eIF4GI and eIF4GII – which are 46 % identical with molecular masses of 171 kDa and 176 kDa, respectively (Gradi et al., 1998). In addition, DAP-5 (p97) and Paip1 are known relatives of eIF4G that exhibit homology to its sequence (Craig et al., 1998; Levy-Strumpf et al., 1997). The two eIF4A-binding sites in mammalian eIF4G are located in the middle region (eIF4G domain spanning residues 616-1087 in eIF4GI) and in the C-terminal region (spanning residues 745-1003) (Imataka and Sonenberg, 1997; Lamphear et al., 1995). Kinetic

binding experiments using surface Plasmon resonance (SPR) have revealed that eIF4A dissociates faster with the central than the carboxy-terminal binding site, thus suggesting that eIF4A binds cooperatively to eIF4G (Morino et al., 2000). The middle regions of eIF4GI and eIF4GII have also been shown to contain a binding site for eIF3 (Imataka and Sonenberg, 1997; Lamphear et al., 1995). Interestingly eIF4GI mutants that are incapable of binding to eIF4A, retain their eIF3-binding activity (Gingras et al., 1999b), Consequently, the binding of eIF3 and eIF4A to MIF4G are thought to be independent interactions (Lamphear et al., 1995).

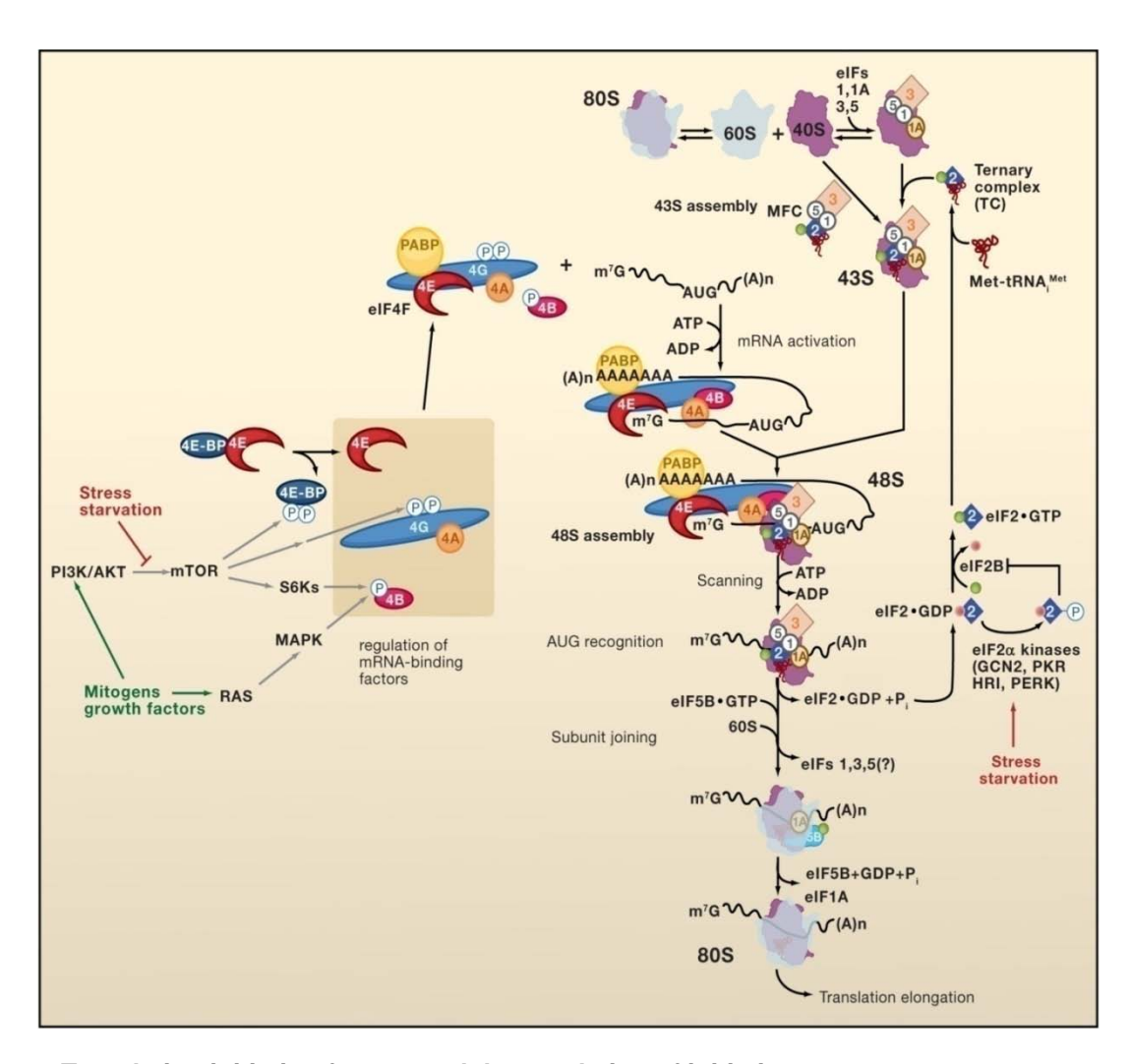


Figure 2 Translation initiation factors and the regulation of initiation (Sonenberg and Hinnebusch, 2009). Numerous initiation factors are involved in the regulation of cap-dependent translation initiation.

Ribosome associated protein eIF3 is multi-subunit complex that stabilizes the binding of eIF2-GTP and Met-tRNAi to the 40S ribosome; prevents the formation of the 80S ribosome by impeding the joining of the 40S ribosome to the 60; and establishes a critical link between the mRNA and the ribosome via its specific interaction with the middle domain of eIF4G (Gingras et al., 1999b; Hinnebusch, 2006; Lamphear et al., 1995; Ohlmann et al., 1996). The recent discovery of other eIF3 binding partners adds another layer to its biochemistry, suggesting that it may also play a role in the stimulation of translation (Derry et al., 2006; Martineau et al., 2008). eIF3 is the largest of the eukaryotic translation initiation factors, and is composed of thirteen subunits with molecular weights ranging from 35 to 170kDa (Hannig, 1995).

#### 1.4. The closed loop model of mRNA translation

The closed loop model of mRNA translation was proposed long before the underlying protein interactions were resolved (Jacobson and Favreau, 1983; Palatnik et al., 1984). The 3'poly(A) tail, which is universal to all eukaryotic mRNAs with the exception of histones, is also thought to be essential in this stimulatory role of translation, functioning as a ribonucleoprotein (RNP) with PABP. Early experiments comparing the translatability, degradation and assembly of synthetic poly(A)<sup>+</sup> and poly(A)<sup>-</sup> mRNAs into messenger RNPs have demonstrated two- to threefold translational stimulation (Munroe and Jacobson, 1990). The cap structure is also a strong determinant of translation efficiency, however, it has been shown that a more potent cooperation results due to a synergy created by joining of the cap structure and poly(A)-tail (Gallie, 1991; Kahvejian et al., 2001). Electroporation of luciferase mRNAs into cells demonstrated that mRNAs, possessing a 5' cap structure and a poly(A) tail were translated more efficiently than mRNAs that lacked those features (Gallie, 1991). Moreover, synergism was also demonstrated in animal, plant and yeast cells possessing capped and polyadenylated mRNAs (Svitkin and Sonenberg, 2006). The

physical interaction of the head and the tail, brought about by the interaction of elF4G and PABP, provides an explanation for translational control via the synergistic effect.

PABP is a multi-domain protein that stimulates translation of mRNAs that have a poly(A) tail. A number of studies in yeast have implicated PABP in mediating the stimulatory effects of translation initiation. The depletion of PABP in yeast, by promoter inactivation or temperature sensitive mutations, has demonstrated a reduction in translation initiation and cell growth (Sachs and Davis, 1989). Moreover, deletion of the Pab1 gene has been shown to be lethal in yeast (Sachs et al., 1987). PABP is abundant in the cell (Gorlach et al., 1994) and coats the poly(A) tail by binding via four phylogenetically conserved tandem RNA recognition motifs (RRMs 1-4) located in the N-terminus tethering it the poly(A) tail (Adam et al., 1986). The RRM is the most common and most studied RNA binding domain as it plays important roles in sequencespecific RNA binding (Clery et al., 2008; Nagai et al., 1995; Perez-Canadillas et al., 2000). This is exemplified by PABP, where RRM 1 and 2 bind the poly(A) tail with high specificity. PABPs interaction with cap bound eIF4G brings about the circularization of the mRNA (Imataka et al., 1998). This is supported by evidence from atomic force microscopy experiments which demonstrated the formation of RNA circles when yeast PABP, eIF4E, eIF4G and a capped and envlated mRNA are mixed (Wells et al., 1998). Consequently, a combined cooperative network created as a result of the interaction of eIF4G with PABP enhances the affinity of eIF4E to the 5'cap facilitating the stable circularization of the mRNA (Figure 3) (Craig et al., 1998; Haghighat and Sonenberg, 1997; Imataka et al., 1998).

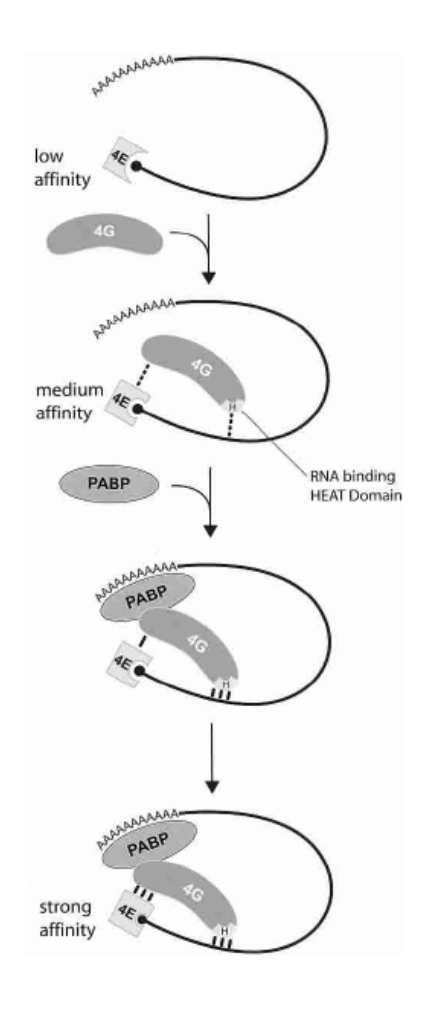


**Figure 3 The closed loop model of mRNA (Svitkin and Sonenberg, 2006).** eIF4E is limits the process of translation initiation and binds the cap weakly. eIF4G binding to the mRNA and PABP enhances the affinity of eIF4E to the 5' cap structure. The 5' cap-eIF4E- eIF4G-PABP-3' poly(A) interaction closes the mRNA loop stabilizing the interaction eIF4E with the complex.

Studies on PABP have demonstrated that PABP fragments can individually stimulate translation independent of their poly(A) binding activity. Interestingly, an RRM 1/2 fragment of PABP, which binds eIF4G, is more effective than full length PABP in translational stimulation (Gray et al., 2000). Moreover, an RRMs 3/4 fragment is still able to stimulate translation although to a lesser degree than the RRM 1/2 fragment. Furthermore, exogenous PABP has been shown to stimulate translation in poly(A)<sup>+</sup> and, to a lesser extent, in poly(A)<sup>-</sup> mRNAs. These findings indicate that PABPs stimulation mechanism is quite complex and may involve alternative pathways (Kahvejian et al., 2001). In light of these results, PABP has been implicated in the

promotion of the recycling of terminating ribosome's by interacting with eIF4F and eRF3 (Hosoda et al., 2003; Imataka and Sonenberg, 1997) and the stimulation 60S subunit joining (Kahvejian et al., 2005; Yoshida et al., 2006), thus outlining two further mechanisms of its translational stimulation capacity.

#### 1.5. PABP-Interacting Proteins 1 and 2 (Paips)

Two PABP interacting partners have been discovered in the search for PABP partners. RRMs 1/2 and the C-terminal domain of PAPB (PABPC) contain binding sites for PABP interacting proteins (Paips) which have been shown to regulate its activity (Berlanga et al., 2006; Craig et al., 1998; Khaleghpour et al., 2001a; Kozlov et al., 2001). The identification of Paips as PABP partners represents the first known mechanism for modulating PABP translational activity, thus flagging another mechanism of controlling translational rates. Paip1 and Paip2A/B act antagonistically, enhancing and repressing translation respectively (Craig et al., 1998; Khaleghpour et al., 2001b). Paip1, Paip2A and Paip2B bind to PABP using two distinct PABP binding motifs, PAM1 and PAM2 (Figure 4). PAM1 is an acidic rich region of about 25 amino acids that binds to RRM1/2 in the N-terminus of PABP. PAM2 is another conserved region that binds the PABC domain (Khaleghpour et al., 2001a; Kozlov et al., 2001). The PAM2/PABC interaction has been shown to play various roles in protein interactions in a number of cellular processes.

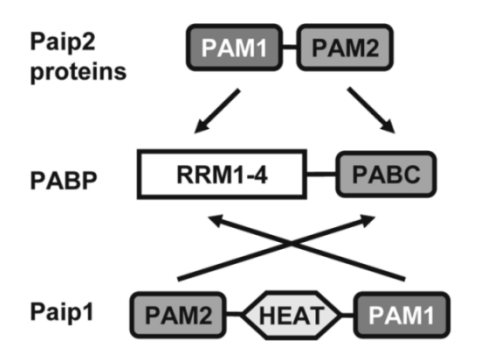


Figure 4 Structural organization and interactions of PABP and Paips (Derry et al., 2006). PAM: PABP-interacting motifs; RRM: RNA recognition motif and PABC: PABP carboxy-terminal domain.

#### 1.6. Paip1

Paip1 is a 54kDa protein of 479 residues that exists in three isoforms; p65, p51 and p45. Paip1 was first discovered as a PABP binding protein that stimulates translation of luciferase reporter mRNA in COS-7 cells (Craig et al., 1998). Deletion of the C-terminal of Paip1, which contains the PAM1 motif, abrogated its ability to enhance translation; thus suggesting that PAM1 is essential for its activity. PAM1 spans residues 440-479 while PAM2 spans residues123-137 (Roy et al., 2002). As previously mentioned, PAM1 and PAM2 motifs mediate the binding of Paip1 to PABP bringing about an interaction of 1:1 stoichiometry (Roy et al., 2002). PAM1 has been shown to exhibit a higher affinity to PABP than to PAM2 (Roy et al., 2002).

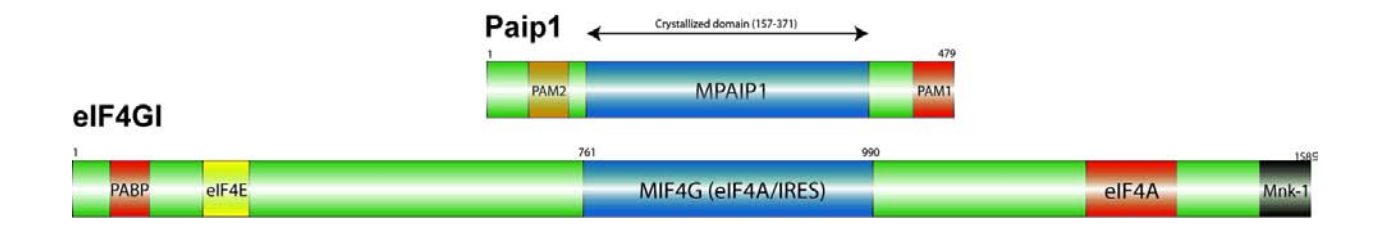


Figure 5 Structural organization of motifs common between Paip1 and eIF4G1.

Schematic alignment of the amino acid sequences of Paip1 and eIF4G1, highlighting conserved protein binding motifs. The interaction between PABP and Paip1 is mediated by two separate PABP-binding motifs (PAM1 and PAM2) located at either end of Paip1 (Roy et al., 2002). PAM1 is an acidic rich region that spans residues 440-479 and binds to the N-terminal RRM2 region of PABP, whereas PAM2 spans residues 123-137 and binds the PABC domain of PABP (Kozlov et al., 2004). The central region of Paip1 (MPaip1; residues 157-375) exhibits 21% identity to the middle domain of eIF4G (MIF4G) and therefore may possess a similar structure. MIF4G is a HEAT domain consisting of five consecutive anti-parallel helix-turn-helix motifs forming a right-handed superhelical structure (Marcotrigiano et al., 2001). This region in eIF4G harbors binding sites for both eIF4A and eIF3 (Imataka and Sonenberg, 1997; LeFebvre et al., 2006). Immunoprecipitation experiments have suggested that Paip1 can also bind to eIF4A and eIF3 (Craig et al., 1998; Martineau et al., 2008).

Paip1 exhibits 39% similarity and 21% identity to the middle sequence of eIF4G (MIF4G residues 761-990. Consistent with the homology between MIF4G (which contains binding sites for eIF4A and eIF3) and the middle domain of Paip1 (MPaip1), Paip1 was coimmunoprecipitated with eIF4A (Craig et al., 1998). However, the residues implicated in the Paip1/ eIF4A interaction have not yet been outlined and not much

information on the affinity is known. Moreover, utilizing GST pull-down experiments using HeLa extract, an interaction between Paip1 and eIF3 has been shown to be specific and RNA independent (Martineau et al., 2008). Paip1 residues spanning 116 to 143 were implicated in binding the G subunit of eIF3. It was also demonstrated that ternary complexes composed of Paip1-PABP-eIF4G and Paip1-eIF3-eIF4G can form in vitro. Overall, the simultaneous interaction of Paip1 with PABP, eIF3 and eIF4A facilitates the bridging of the 5' cap and the 3' poly(A) tail of mRNA (Figure 6).

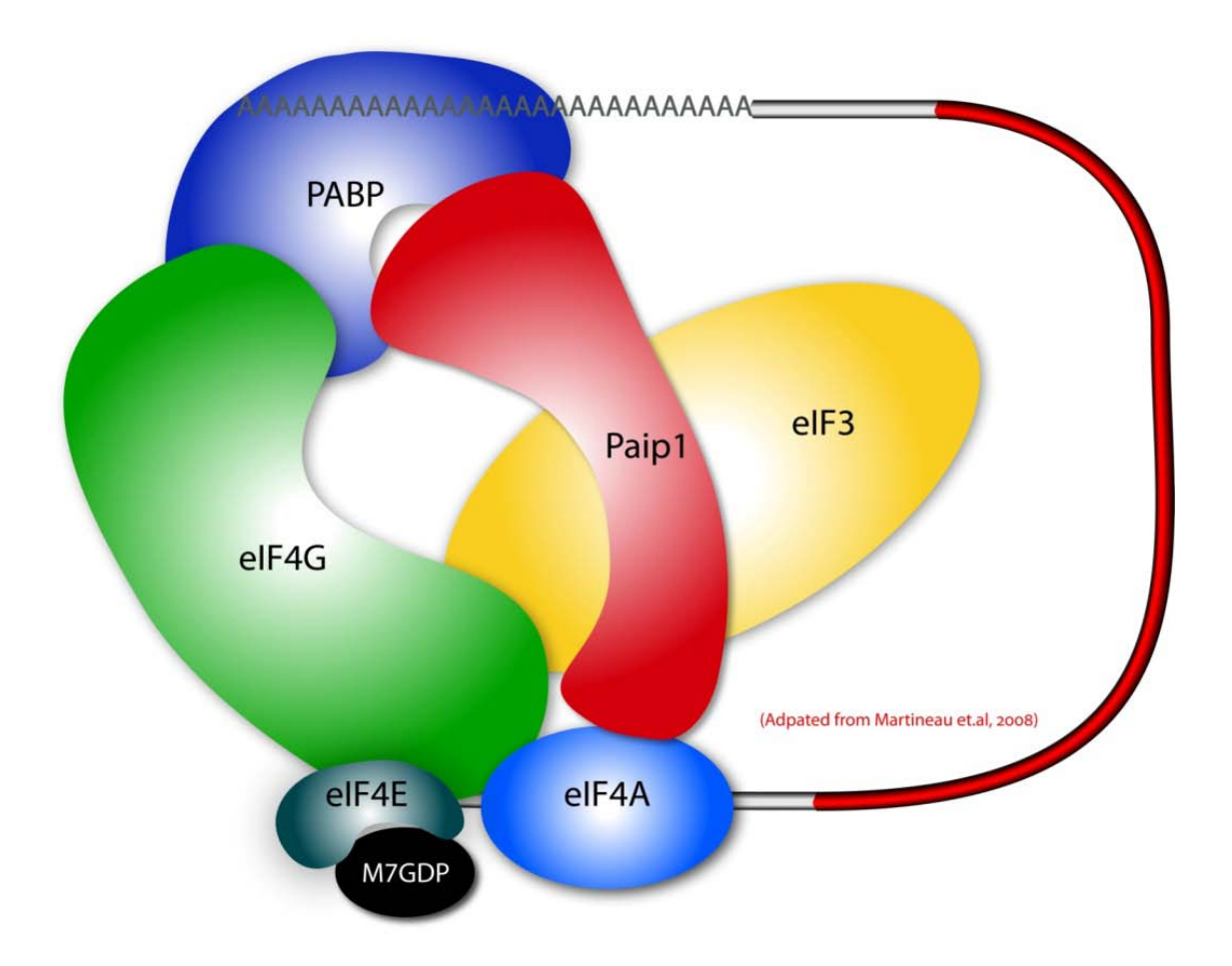


Figure 6 Model of Paip1 enhancement of Translation.

eIF4F is a three subunit complex composed of cap-binding protein eIF4E, a DEAD-box helicase eIF4A and multi-scaffolding protein eIF4G (Gingras et al., 1999b). eIF4G bridges eIF4A and eIF4E, allows the circularization of mRNA by interacting with PABP and recruits the 43S ribosome by interacting with eIF3. Paip1 has been shown to interact with eIF3, eIF4A and PABP. The interaction of Paip1 with eIF3 is direct and independent of mRNA and as result is postulated to regulate Paip1 activity (Derry et al., 2006). The simultaneous interaction of Paip1 with PABP, eIF4A and eIF3 facilitates and stabilizes the circularization of mRNA, thus enhancing translational rates.

#### 1.7. Paip1 implicated in mRNA turnover

In addition to translational stimulation, Paip1 has been show to be involved in mRNA turnover. Several studies have reported a link between mRNA translation and mRNA decay, with the latter thought to be dictated by certain sequence elements located within protien-coding regions (Shyu et al., 1989; Wisdom and Lee, 1991). The role of translation in mRNA turnover has been established using the c-fos mRNA as a model system. Two destabilizing regions within the c-fos protein coding region - termed protein-coding region determinants of instability (CRD-1 and CRD-2) have been identified (Chen et al., 1992). CRD-1 is the major determinant of instability and is referred to as the mCRD (Chen et al., 1992). mCRD associates with the mRNA to direct accelerated deadenylation thus causing its degradation (Grosset et al., 2000). This activity is regulated by five protein complex that bridges the mCRD to the mRNA. Paip1 and PABP are subunits of this complex which also includes Unr, a purine-rich RNA binding protein; hnRNP D, an AU-rich element binding protein; and NSAP1, an nhRNP R-like protein (Grosset et al., 2000). The bridging complex that exists between the mRNA and the poly(A) tail prevents deadenylation by stabilizing the poly(A) tail. During translation, ribosomal movement across the mCRD disrupts the bridging complex, thus allowing the formation of metastable structures which expose the poly(A) tail to nuclease attack resulting in mRNA decay. In this manner, Paip1 functions as an mRNA decay protection factor.

# 1.8. Pathological relevance of Paip1 in familial Amyotrophic lateral sclerosis (FALS) and Cervical Cancer (CC)

It has also been suggested that Paip1 may be related to the pathogenesis of familial Amyotrophic lateral sclerosis (FALS). Amyotrophic lateral sclerosis (ALS) is a neurodegenerative disease characterized by progressive muscular paralysis causing the degeneration of motor neurons in the primary motor cortex, spinal tracts, brainstem and spinal cord (Wijesekera and Leigh, 2009). Approximately 10% of all ALS cases are inherited. 20% of cases accorded to the familial form of ALS have been associated with mutations in the Cu/Zn superoxide dismutase (SOD1) gene (Ince et al., 1998; Pasinelli and Brown, 2006; Rosen, 1993). Several explanations have been postulated for the mechanism by which SOD1 mutations cause selective motor neuron death, however, the underlying mechanism remains elusive. It is understood that the damage within motor neurons expressing mutant SOD1 causes disease onset, whereas damage within their glial cell neighbors expressing mutant SOD1 accelerates disease progression (Yamanaka et al., 2008). In a study aimed at uncovering related molecules bringing about the pathologic mechanisms of FALS, gene expression in the spinal cord of Leu126delTT mutated SOD1 transgenic mice (TgM) was investigated. Immunohistochemical analysis revealed abnormal levels of four proteins specific to the SOD1 mutant, of which Paip1 was one (Fukada et al., 2007). Utilizing histopathological and immunohistochemical assays, Paip1 was detected in the cytoplasm of microglial cells in transgenic mice (TgM) -at-onset and in post-symtomatic TgM (Fukada et al., 2007). It has been suggested by other reports that a mutation in SOD1 (G93A) of the neuroprotective microglial cells results in neurotoxicity (Beers et al., 2006). Consequently, upregulation of Paip1 in the early phase of FALS may be an early indicator of microglial activation. This suggests that Paip1 is related to the pathogensis of FALS and as a result, may have implications for the assessment of ALS progression or its diagnosis (Fukada et al., 2007).

In addition to FALS, Paip1 has also been implicated in cervical cancer (CC). CC tumours are a major cause of cancer death in women, progressing by distinct morphological changes from normal to carcinomitous epithelia (Waggoner, 2003). To date, no biological or genetic markers are known to predict the likelihood of lesion progression from precancerous to invasive CC. Copy number gains and amplification of chromosomes are a characteristic feature of cancers, with gain of short arm of chromosome of 5 (5p) being the most frequent karyotypic change in CC (Schwab, 1999). In an integrative genomic approach, utilizing a combination of single nucleotide polymorphism (SNP) array, fluorescence in situ hybridization (FISH) and gene expression analysis on various stages of CC progression, Scotto et al. have identified several transcriptional targets of 5p gain. SNP and FISH revealed a copy number increase (CNI) of 5p in invasive CC (Scotto et al., 2008). Moreover, gene expression analysis identified several 5p genes that play a role in DNA repair and cell cycle regulation, including Paip1, as targets of CNI (Scotto et al., 2008). The identification of Paip1 as a 5p gene target in CC denotes the possibility of its use as biomarker or a molecular therapeutic target (Scotto et al., 2008).

#### 1.9. Regulation of Paip Proteins

Little is known on how Paips are regulated other than they are subject to ubiquitin mediated degradation. By covalent linkage to ubiquitin, substrates are marked for degradation by the ubiquitin–proteasome degradation pathway (Glickman and Ciechanover, 2002; Hershko and Ciechanover, 1998; Hochstrasser, 1996). In general, ubiquitination requires the ubiquitin activating enzyme (E1); the ubiquitin-carrier or conjugating enzyme (E2); and the ubiquitin ligase (E3) which transfers activated ubiquitin to the protein substrate (Hershko and Ciechanover, 1998; Pickart and Rose, 1985). The ubiquitinated substrates are then recognized and degraded by the 26S proteasome. Interestingly, the sequence spanning the PABC domain of PABP, which

interacts with PAM2 of Paips, is also present in the C-terminal of the E3 ubiquitin-protein ligase EDD (human orthologue of the hyperplastic disc protein), a member of Homologus to E6-AP Carboxyl-terminus (HECT) domain family (Callaghan et al., 1998; Huibregtse et al., 1995; Oughtred et al., 2002). Accordingly, it was demonstrated the Paip2A and Paip2B are ubiquitinated upon transfection into cells (Berlanga et al., 2006). However, the PABC domain of EDD is missing the first  $\alpha$ -helix conferring a weaker affinity to Paip2A. Consequently, under physiological conditions, the higher affinity of Paip2A to PABP serves to regulate its degradation by EDD-dependent proteolysis (Yoshida et al., 2006). Once PABP levels decline, Paip2A is free to associate with EDD and is subsequently degraded by the proteasome following ubiquitination. Similarly, the PABC domain of hyperplastic discs protein (HYD) in *Drosophila melanogaster* has been shown to interact with Paip1 (Deo et al., 2001). However, depleting PABP levels in the cell does not result in the degradation of Paip1, indicating that it may require additional and unknown factors in degradation.

It has also been suggested that the independent and direct interaction of eIF3 with Paip1 may function as a mechanism of regulation (Derry et al., 2006; Martineau et al., 2008). This view is backed by experiments which showed that the stimulation of cells with serum, insulin or Epidermal growth factor results in increased binding of eIF3 to Paip1; and the addition of mTOR, MEK1/2 or PI3K inhibitors caused a decrease in binding (Derry et al., 2006; Martineau et al., 2008). Additionally, upon cotransfecting cells with siRNA to eIF3a, Paip1-dependent enhancement was abrogated. This suggests that eIF3 regulates Paip1 activity by extension of the MAPK and mTOR pathways. Therefore, eIF3 employs Paip1 as a proxy to control PABP activity and translational rates (Derry et al., 2006). Other potential mechanisms of Paip1 regulation may exist via binding to other yet unknown ligands.

#### 1.10. Structure of MIF4G homologs

MIF4Gs share a common structure but can differ in sequence. The MIF4G domain is a structural motif with a HEAT-repeat-type fold, consisting of a 2-layer alpha/alpha right-handed superhelix (Aravind and Koonin, 2000). MIF4G domains are found in several proteins involved in RNA metabolism, including eIF-2b, a translation initiation factor; UPF2 a regulator of nonsense transcripts 2 (Kadlec et al., 2004); and the nuclear cap-binding proteins CBP80, CBC1, NCBP1, although sequence identity between them may be low (Kim et al., 2009).

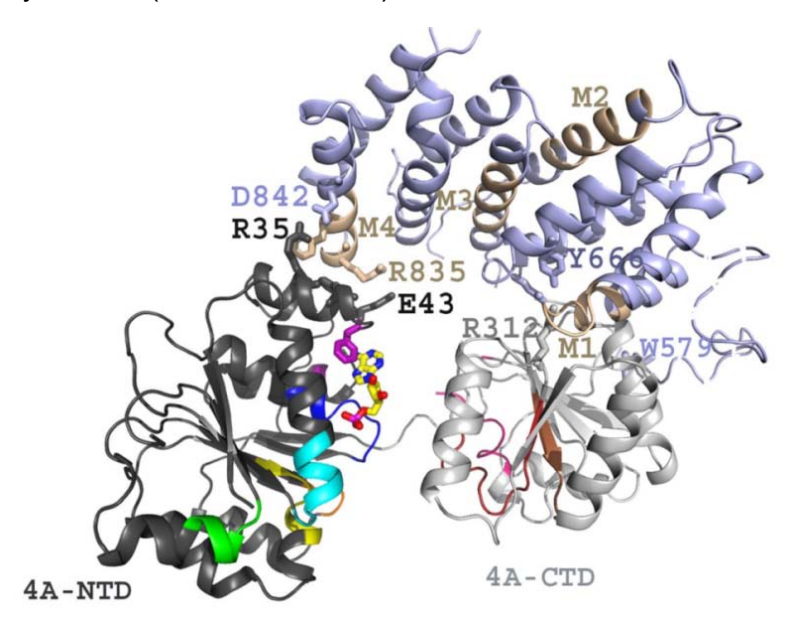


Figure 7 Crystal structure of the yeast eIF4A-eIF4G complex highlighting the key Trp residue (W579) (Schutz et al., 2008).

The structures of two MIF4G domains have already been determined in homo sapiens eIF4GII (Marcotrigiano et al., 2001) and Saccharomyces cerevisiae eIF4GI (Schutz et al., 2008). The structures revealed a crescent shaped molecule that belongs to the HEAT-repeat family of protein, which is generated by five repeating pairs of antiparallel  $\alpha$ -helices stacked upon each other. The latter group determined the structure of eIF4GI in complex with eIF4A highlighting three contiguous interaction surfaces including a key tryptophan residue that bolsters the interaction (Figure 7) (Schutz et al., 2008). The significance of the tryptophan residue was demonstrated by

shortening of the eIF4G sequence at the N-terminal which resulted in significant loss of its eIF4A binding affinity (Schutz et al., 2008). This result was also confirmed via site-directed mutagenesis and pull-down experiments. The two other contiguous interaction surfaces involved the N-terminal and C-terminal regions of MIF4G which contacted the C-terminal and N-terminal regions of eIF4A, respectively. Overall, the interface between MIF4G and eIF4A contains 23 hydrogen bonds and 14 salt bridges.

#### 1.11. Aims of the study

The information stated above demonstrates the important role of Paip1 in the stimulation of translation and mRNA turnover. Its implication in FALS and CC renders it a possible target in pharmaceutical therapy. The objective of this study is to solve the structure of Paip1 and analyze its uncharacterized interaction with eIF4A.

#### 2. MATERIALS AND METHODS

#### 2.1. MATERIALS

#### 2.1.1. Chemicals

All chemicals used were of quality pro analysi. Solutions were prepared with deionized, double-distilled and sterile-filtered water. Concentrations in percent of liquids are given as (v/v) and of solid chemicals as (w/v).

Acrylamide, Bioshop Canada Inc, Burlington, ON

Ampicilin, Bioshop Canada Inc, Burlington, ON

Agarose (UltraPure™), *Invitrogen*, Barcelona, Spain

Biotryoptone, Bioshop Canada Inc, Burlington, ON

Coomassie Brilliant Blue R-250, BioRad Laboratories, Hercules, C

DTT, Bioshop Canada Inc, Burlington, ON

Dextrose, ACP Chemicals Inc, Montreal, QC

Glacial Acetic Acid, Fischer Scientific, Nepean, ON

Glycerol, Fischer Scientific, Fairlawn, NJ

Glutathione, GE Healthcare, Uppsala, Sweden

Imidazole, Bioshop Canada Inc, Burlington, ON

IPTG, Bioshop Canada Inc, Burlington, ON

α-Lactose monohydtrate, Sigma Aldrich, Steinheim, Germany

β-ME, Bioshop Canada Inc, Burlington, ON

MES, Bioshop Canada Inc, Burlington, ON

Methanol, Fischer Scientific, Fairlawn, NJ

PEG 20,000, Fluka BioChemika, Deisenhofen, Germany

TCEP, Bioshop Canada Inc, Burlington, ON

TEMED, Bioshop Canada Inc, Burlington, ON

TRIS, Bioshop Canada Inc, Burlington, ON

Yeast extract, Bioshop Canada Inc, Burlington, ON

X-gal, Bioshop Canada Inc, Burlington, ON

#### 2.1.2. Buffers, solutions and Kits

QIAprep Spin Miniprep Kit, QIAGEN Sciences, Germantown, MD

Buffer P1: 100 µg/ml RNase A, 50 mM Tris-HCl pH 8.0, 10mM EDTA.

Buffer P2: 200 mM NaOH, 1% (w/v) SDS

Buffer N3: 3 M NaCl, 11.5% (v/v) Glacial acetic acid.

Buffer PE: 70% (v/v) ethanol.

Buffer EB: 10 mM Tris-HCl, pH 8.5

Precission Plus Protein standard, Bio-Rad, Hercules, USA

**SDS-PAGE Staining solution**: 2 g/l Coomassie Brilliant Blue R-250, 25% (v/v) ethanol, 10% (v/v) glacial acetic acid, 65% (v/v) Water.

**SDS-PAGE Destaining solution**: 25% (v/v) ethanol, 10% (v/v) glacial acetic acid, 65% (v/v) Water.

**NiA Wash Buffer**: 25 mM Tris-HCl pH 8.0, 500 mM NaCl, 5% glycerol and 10 mM lmidazole.

**NiB Elution Buffer**: 25 mM Tris-HCl pH 8.0, 500 mM NaCl, 5% glycerol and 500 mM Imidazole.

**QA Wash Buffer**: 20 mM Tris-HCl pH 8.0, 50 mM NaCl and 5% glycerol.

**QB Elution Buffer**: 20 mM Tris-HCl pH 8.0, 500 mM NaCl and 5% glycerol.

**QD Dilution Buffer**: 20 mM Tris-HCl pH 8.0 and 5% glycerol.

**GF Buffer**: 50 mM Tris-HCl pH 8.0, 150 mM NaCl and 5% glycerol.

#### 2.1.3. Cell growth media

#### Luria Bertani (LB) medium

10 g/L Biotryptone, 5 g/L yeast extract and 5 g/L NaCl. The mixture is dissolved in 990 ml of water and autoclave sterilized.

#### LB agar

15 g/L agar is added to the LB mixture. The mixture is dissolved in 990 ml of water, autoclave sterilized, allowed to cool to 45 °C and supplemented with the appropriate antibiotics before pouring plates.

#### M9 medium

5X M9 salts component stock is composed of 64 g/L Na<sub>2</sub>HPO<sub>4</sub>.7H<sub>2</sub>O, 15 g/L KH<sub>2</sub>PO<sub>4</sub>, 2.5 g/L NaCl and 5 g/L NH<sub>4</sub>Cl.

To make 1X M9 media, 200 ml of 5X M9 salts component stock is added to 800 ml of water and autoclave sterilized. 5 g/L glucose, 100  $\mu$ l/L CaCl<sub>2</sub> (1M), 1 ml/L MgSO4 (2M), 2 mg/L biotin and 2 mg/L thiamine is added to the medium at the expression stage.

#### ZYM-5052 Auto-Inducing medium (Studier, 2005)

10g/L Bactotryptone, 5g/L Yeast extract, 20 ml/L 50X M component stock, 20ml/L 50X 5052 component stock and 1 ml/L MgSO4 (2M). The mixture was dissolved in 990 ml of water and autoclave sterilized.

50X M component stock is composed of 177.5g/L Na2HPO4, 170.3g/L KH2PO4, 107g/L NH4Cl, 33g/L (NH<sub>4</sub>)<sub>2</sub>SO4, and 50X 5052 component stock is composed of 25g/L Dextrose 250ml/L Glycerol, 100g/L  $\alpha$ -Lactose monohydrate.

#### 2.2. METHODS

#### 2.2.1. General Procedures

#### Miniprep

The QIAprep® miniprep kit was used for the purification of plasmid DNA from overnight *Escherichia coli* (BL21or DH5a) cultures in LB medium. The procedure is based on the modified alkaline lysis of bacterial cells method (Birnboim and Doly, 1979), followed by the adsorption of DNA onto silica in a high salt solution (Vogelstein and Gillespie, 1979).

Pelleted bacteria are resuspended in  $250\mu l$  of P1 buffer and lysed with the same amount of P2 buffer. As a result, the solution contains SDS, RNase A and an alkaline environment, which act by lysing the cells, degrading RNA (which could contaminate the DNA prep) and denaturing proteins and DNA, respectively. The lysate is then neutralized with  $350\mu l$  of high salt N3 buffer, which causes the renaturation of plasmid DNA and the precipitation of all other components. The resulting plasmid containing solution is loaded onto a QIAprep spin column containing the DNA adsorbent silica membrane.  $750\mu l$  PE buffer is used to wash all other extraneous debris before final elution with  $50\,\mu l$  of water or EB buffer.

#### **DNA** sequencing

All coding sequences of plasmid constructs were confirmed at the McGill University and Génome Québec Innovation Centre sequencing service.

#### Agarose gel electrophoresis

Agarose gel electrophoresis is a method used to estimate the size of DNA molecules following PCR and restriction enzyme digestion. Samples are prepared using 1-2  $\mu$ l of DNA and 5-7  $\mu$ l of 6X loading buffer which are loaded onto 1% agarose gels (prepared

in Tris/Borate/EDTA buffer; TBE) supplemented with the 1  $\mu$ l of ethidium bromide. An appropriate amount of DNA ladder is also loaded for estimation of DNA size. Electrophoresis is carried out at a constant voltage of 100V in TBE buffer and an ultraviolet Transilluminator is then used to visualize the ethiduim bromide stained DNA.

#### **Standard Transformation Protocol**

Competent cells frozen at -80°C are first thawed gently on ice for a period of five minutes. 1µI of DNA is added to 50 µI of competent cells followed by a 15-20 minute incubation period on ice. The cells are then heat shocked at 42°C for 30s and kept on ice for 2 minutes. 700 µI of LB are then added to the reactions which are subsequently incubated at 37°C in shaker for 1 hour. The transformation reactions are then plated on LB-agar plates treated with the appropriate antibiotic and incubated in a 37°C chamber for 12-16 hours overnight.

#### Sodium Dodecyl Sulfate Polyacrylamide Gel Electrophoresis (SDS-PAGE)

SDS-PAGE is a method used to analyze protein purification fractions chromatographically, under denaturing, reducing conditions. Samples are prepared using 10-15 µl of fraction sample and 25-30 µl of 2X loading buffer. The samples are incubated for a period of 5-10 mins at 95°C before loading on the polyacrylamide gels. 5-6 µl of Precission Plus protein standard is also loaded for mass comparison of protein size. Electrophoresis is carried out at a constant voltage of 230V in SDS buffer, followed by a 30-60 minute staining period in SDS-PAGE staining solution and overnight destaining in SDS-PAGE destaining solution buffer.

#### 2.2.2. Paip1 and elF4A Plasmid preparation

Four Paip1 (homo sapiens) constructs were generated for expression as hexahistidine fusion proteins. Paip1(FL), Paip1(154-375), Paip1(157-375) and Paip1(154-479) were **PCR** 5'amplified by using primers paip1 forward GGGGGGGATCCATGTCGGACGGTTTCGATCGG -3', paip1 reverse 5'-GGGGGGAATTCTTACTGTTTTCGCTTACG-3'; paip1(154-375) forward 5'-GAGGATGGATCCGAGGATTATCCTACTCTATCA-3', paip1(154-375) reverse, 5'-GACTCTGAATTCTTAACTTGACCGGAGTTCTACAAG-3'; paip1(157-375) forward 5'-GAGGATGGATCCACTCTATCAGAATATGTTCAG -3'; paip1 (157-375) reverse 5'-GACTCTGAATTCTTAACTTGACCGGAGTTCTACAAG -3', paip1(154-479) forward 5'-GAGGATGGATCCGAGGATTATCCTACTCTATCA -3' and paip1(154-479) reverse 5'-GGGGGGAATTCTTACTGTTTTCGCTTACG-3' in order to introduce BamH1 and EcoRI restriction sites. The purified PCR products were digested with BamH1 and EcoRI restriction enzymes and ligated into the BamH1-EcoRI site of the expression vector pPROEX-HTb. The recombinant plasmids were transformed into E. coli BL21(DE3) for inducible expression as hexahistidine fusion proteins. eIF4A (FL) was generated for expression also as a hexahistidine tagged fusion protein using the same method with the primers eIF4A forward 5'- GGG GGG GGA TCC ATG TCT GCG AGC CAG GAT-3' and eIF4A reverse 5'- GGG GGG GAA TTC TCA GAT GAG GTC AGC AAC-3'.

# 2.2.3. Protein expression of Paip1 plasmids; Paip1, Paip1 (157-371), Paip1 (154-371) and Paip1 (154-479)

Paip1(FL), Paip1(157-371), Paip1(154-371) and Paip1(154-479) plasmids were transformed into the BL21 (DE3) *E.Coli* strain according the standard transformation protocol (described above), plated on LB-Agar plates treated with 100 μg/ml of Ampicillin and incubated for at 37°C for 14-16 hours. Single colonies were injected into

a 100 ml LB starter culture treated with 100 μg/ml of Ampicillin. The starter cultures were incubated at 37°C for 14-16 hours shaking at 210 rpm followed by a 10X dilution to 1L. Bacteria were then induced for protein production using isopropylthiogalactopyranoside (IPTG) at a final concentration of 1 mM once OD600nm of 0.6 was reached. For efficient protein production the incubation temperature was then lowered to 30°C and incubation was sustained at 210 rpm for another 4 hours. The cells were then harvested by centrifugation for a period of 15 minutes at 3000 rpm (2264g). The supernatant was discarded and the pellets were resuspended in 20-30 ml of NiA Buffer. The cells were either flash frozen using liquid nitrogen and stored at -80°C; or lysed by two passes through a French press High-Pressure Homogenizer (Avestin) in NiA buffer to commence purification. Cells were usually expressed in 4L batches to produce protein in mg quantities for crystallization, pulldown, ITC and SPR experiments.

#### 2.2.4. Protein expression of Se-Met Paip1(157-371)

To solve the phase problem via anomalous dispersion methods, methionine was substituted for selenomethionine by the methionine biosynthesis inhibition pathway (Doublie, 1997). Paip1(157-371) BL21 (DE3) colonies were injected into 1 ml of LB starter culture treated with 100 μg/ml of Ampicillin. The culture was grown at 37°C shaking at 210 rpm for a period of 8 hours followed by centrifugation at 3000 rpm (2264g) for a period of 5 minutes. Pellets were resuspended in 1ml of 1X M9 medium followed by dilution into 100 ml of 1X M9 medium treated with 100 μg/ml of Ampicillin. The M9 culture was cultivated for a period of 14-16 hours, followed by a 10X dilution into 1L of 1X M9 medium supplemented with 5 g/L glucose, 100 μl/L 1M CaCl<sub>2</sub>, 1 ml/L 2M MgSO4, 2 mg/L biotin, 2 mg/L thiamine and 100μg/ml of Ampicillin. Upon reaching an OD<sub>600nm</sub> of 0.6, 100 mg/L of L-Lys, L-Phe, L-Thr and 50 mg/L of L-Ile, L-Let, L-Val and L-Se-Met were supplemented and allowed to dissolve for a period of 10 minutes. The cultures were then induced with IPTG at a final concentration of 0.8 mM where the

temperature was lowered to 30°C to facilitate protein expression. The cultures were harvested by centrifugation for a period of 15 minutes at 3000 rpm (2264g). The supernatant was discarded and the pellets were resuspended in 20-30ml of NiA Buffer. The cells were either flash frozen using liquid nitrogen and stored at -80°C; or lysed by two passes through a French press High-Pressure Homogenizer (Avestin) in cold lyses buffer containing 25 mM Tris-HCl pH 8.0, 500 mM NaCl, 5% glycerol and 10 mM imidazole to commence purification. Cells were usually expressed in 5L batches to produce protein in mg quantities for crystallization experiments.

#### 2.2.5. Protein expression of recombinant eIF4A

Full length hexahistidine tagged eIF4A plasmid was transformed into the BL21 (DE3) E.Coli strain according the standard transformation protocol, plated on LB-Agar plates treated with 100  $\mu$ g/ml of Ampicillin and incubated at 37°C for 14-16 hours. Single colonies were injected into 5 ml ZYM-5052 starter cultures treated with 100 $\mu$ g/ml Ampicillin. Starter cultures were incubated at 37°C for 14-16 hours shaking at 210 rpm followed by a 10X dilution to 1L. The temperature was sustained at 37°C for a period of 2-3 hours and was then lowered to 20°C for a period of 20-22 hours to facilitate protein expression. The ZYM-5052 medium utilizes the auto-inducing method of expression (Studier, 2005), thus IPTG was not necessary. The cells were then harvested by centrifugation for 15 minutes at 3000 rpm (2264g). The supernatant was discarded and the pellets were resuspended in 50-60ml of NiA Buffer. The cells were either flash frozen using liquid nitrogen and stored at -80°C; or lysed to commence purification. Cells were usually expressed in 4L batches to produce protein in mg quantities for pulldown assays, ITC and SPR experiments.

#### 2.2.6. Protein Purification

The ÄKTA™purifier (GE Healthcare Life Sciences) was utilized in all purification steps for versatility and use of tailor-made buffer solutions for the specific application of the workflow outline below.

#### 2.2.6.1. Immobilized metal affinity chromatography (IMAC)

Immobilized metal affinity chromatography was first used to purify all Paip1 constructs and eIF4A based on the Ni-affinity of the N-terminal hexahistidine tag (Porath et al., 1975). The supernatant was loaded onto a Ni affinity column (HisTrap 5 ml FF, GE Healthcare) equilibrated with buffer NiA. The loaded column was washed with 5 column volumes of buffer NiA and protein was eluted with a linear gradient of 0-50 % of buffer NiB over a gradient length of 11 column volumes. Samples from peak fractions, cell lysate, the supernatant and the flow-through of the Ni column were analyzed by SDS-PAGE to estimate protein size and to monitor protein solubility and column affinity. Fractions containing the protein samples were pooled and cleaved with approximately 1 mg tobacco etch virus (TEV) protease per 25 mg of crude protein at 4°C while dialyzing overnight against a 2 L buffer of 20 mM Tris(pH 8.0), 100mM NaCl, 0.5 mM DTT and 5 % glycerol with a 3.5 kDa molecular cutoff membrane. Cleaved protein was collected in the flow through of a second bout of Ni-column chromatography.

#### 2.2.6.2. Anion Exchange chromatography (AEC)

To separate the target sample and other impurities according to charge, anion exchange chromatography was performed. Cleaved protein was diluted 10X to minimize salt concentration and loaded onto an anion exchange column (HiTrap Q FF, GE Healthcare) equilibrated with 20 mM Tris pH 8.0, 0.5 mM DTT, 5 % glycerol (QA). The loaded column was washed with 5 column volumes of buffer QA and the protein was

eluted with a linear gradient of 0-50 % buffer QB over a gradient length of 20 column volumes. The peak fractions were analyzed using SDS-PAGE and fractions containing Paip1 constructs or eIF4A were pooled and either frozen in liquid nitrogen for storage at -80 °C or concentrated for size exclusion chromatography.

#### 2.2.6.3. Size-exclusion chromatography (SEC)

As a final purification step, size-exclusion chromatography (gel filtration) was used to separate the proteins in the sample according to their hydrodynamic volume or size. Protein samples were concentrated to final volumes of 500-1000µl and, depending on the calculated size of the construct, were either loaded onto Superdex<sup>™</sup> 75 (GE Healthcare) or Superdex<sup>™</sup> 200 (GE Healthcare) gel filtration columns. The columns were pre-equilibrated with 25 mM Tris-HCl pH 8.0, 200 mM NaCl and 5% glycerol GF buffer. The peak fractions were analyzed using SDS-PAGE. Fractions containing the desired protein sample were concentrated and flash frozen in liquid nitrogen for storage at -80 °C.

#### 2.2.7. Crystallization

Protein crystallization experiments were conducted at two different concentrations of 15 mg/ml and 25 mg/ml. Initial screens were set up using the sitting drop vapour diffusion method on Intelli-Plate<sup>TM</sup> 96x2 well plates utilizing the Art Robbins Phoenix Liquid Handling System. For rapid, practical and effective screening QIAGEN NeXtal suites Classics I, Classics II, Sparse Matrix I, Sparse Matrix II and PEG were used to prepare 480 drops for each protein. The drops were of 1:1 protein to solution ratio, with a final volume of  $0.2\mu l$ . The drops were allowed to equilibrate against  $100 \mu l$  of reservoir solution to allow crystal formation. Successful screens were verified by the hanging drop vapour diffusion method by preparing I  $\mu l$  and 2  $\mu l$  drops on QIAGEN EasyXtal 24 well plates. Conditions that generated reproducible crystals were tested for diffraction at the

McGill X-Ray Home Source (Rigaku rotating copper-anode generator outfitted with Osmic confocal optics and an R-AXIS IV++ image-plate detector). Reproducible conditions that diffracted well were further broken down to construct several conditions of slight component variability in concentration and pH. Selenomethionine protein crystals were setup using the hanging drop vapour diffusion method with slight variability to the final native protein condition.

#### 2.2.8. X-ray diffraction and Data collection

Crystals were initially tested for X-ray diffraction on an in-house Rigaku rotating copperanode generator outfitted with Osmic confocal optics and an R-AXIS IV++ image-plate detector. MAD and SAD data were collected at the selenium absorption edge on SeMet containing crystals on the at the F2 and A1 beamlines at the Cornell High Energy Synchrotron Source (CHESS), Ithaca, New York. Crystals were mounted on a cryogenic loop of the appropriate size and were flash frozen in liquid nitrogen before diffraction. The program HKL2000 (Otwinowski and Minor, 1997) was used for data processing.

#### 2.2.9. Phasing, Model building and Refinement

The program "Solve" (Terwilliger and Berendzen, 1999) was used to obtain the phases from the MPaip1 SeMet SAD data and the program "Resolve" (Terwilliger, 2000) was used for solvent flattening and density modification. The resulting electron density map was traced using the program Coot (Emsley and Cowtan, 2004). Models refinement is currently in progress using the program CNS (Brunger et al., 1998).

## 2.2.10. Small Angle X-ray Scattering (SAXS)

Small-angle X-ray scattering (SAXS) was employed in order to obtain a picture of the overall configuration of the MPaip1 (middle domain of Paip1) directly in solution. SAXS data of MPaip1 were collected using a SAXSess small-and wide-angle X-ray scattering system (Anton-Paar). Protein samples were initially dialyzed overnight in a buffer

containing 50 mM Tris-HCl pH 8.0, 150 mM NaCl and 1mmDTT. Scattering data were collected for MPaip1 and the dialysis buffer to subtract background scattering generated by the buffer. The primary scattering data were desmeared and plotted to obtain the radius of gyration (Rg) via Guinier analysis using the program Primus (Konarev et al., 2003). The distance distribution function was calculated using the program GNOM (Svergun, 1991, 1992). Ten independent shape reconstructions were carried out using the program GASBOR (Svergun et al., 2001) and averaged/filtered to correspond to the expected molecular weight of MPaip1.

#### 2.2.11. Pull down experiments

Pull-down experiments are a screening technique for identification of protein-protein interactions. His-tag pull-down experiments were performed to analyze the binding of Paip1 constructs to eIF4A. 0.5 mg of prey protein (His-eIF4A) were bound to a Ni-NTA-Sepharose resin (acquired from HisTrap FF Column) and incubated for 1 hour. Unbound protein was then washed with a buffer containing 500mM NaCl, 25mM Tris-HCl pH 8.0, 10mM imidazole and 5% glycerol (PD buffer). 1 mg of bait proteins (Paip1 constructs) were then added to react with prey protein and incubated for 1 hour. Bound proteins were then eluted with PD buffer containing 500 mM imidazole.. The eluate was then resolved by SDS-PAGE. To confirm that the basic conditions of the experiment were able to produce a positive result, a positive control reaction was also conducted (eIF4A and eIF4G). To account for non-specific background binding to the beads, bait proteins were loaded onto the column and the same procedure was followed under the same time frame, without the addition of an interacting partner.

#### 2.2.12. Isothermal Titration Calorimetry (ITC)

Isothermal Titration Calorimetry experiments were performed to analyze kinetics of the Paip1/eIF4A binding. Experiments were performed with a VP-ITC instrument (Microcal) at 20 °C. MPaip1 and eIF4A samples were first dialyzed against a buffer containing 50mM Tris (pH 7.5), 100 mM NaCl, 0.5 mM TCEP, 15 % glycerol and then diluted to 0.5-1.0 mM and 0.05-0.1mM respectively. Paip1 constructs were loaded into the syringe while eIF4A was loaded into the cell. The heat of binding was measured over the injection of 37 µl of Paip1 in 2 µl increments into the vessel. Data were fitted to a one binding site model using the Origin software package (Microcal).

#### 2.2.13. Surface Plasmon Resonance (SPR)

In addition to ITC, Surface Plasmon Resonance (SPR) was employed to study the kinetics of the Paip1/eIF4A. SPR analysis was done using a Biacore T100. A Biacore Sensor Chip NTA was used to immobilize the hexahistidine tagged proteins. The running buffer was 10 mM Hepes pH 7.4, 150 mM NaCl, 0.05% P20 surfactant, and 50 µM EDTA. Ni++ was complexed with NTA on the chip surface, prior to protein capture, with a 1 minute pulse of 500 µM NiSO<sub>4</sub> in running buffer. Between experiments the sensor chip surface was stripped of protein (regenerated) using the running buffer supplemented with 0.35 M EDTA. The flow rate was left at 10 µl / min for all binding tests, and the temperature was set at 25°C. Approximately 2000 RU of eIF4A-His (100 µg/ml stock) was captured to flow cell 2, while flow cell 1 was left empty as a control. Untagged Paip1 was injected over flow cells 1 and 2 for 60 seconds at concentrations of 1 nM, 10nM, 100nM and 1 μM. Paip1 dilutions (1 nM - 100 μM, 10 fold series) were also prepared with the addition of 1 mM DTT for 60 second injections over flow cells 1 and 2. In the reverse experiment approximately 1600 RU of His-Paip1 was captured to flow cell 2, while flow cell 1 was left empty as a control. Untagged eIF4A was injected over flow cells 1 and 2 for 60 seconds at concentrations of 1 µM and 10 µM.

#### 3. RESULTS AND DISCUSSION

### 3.1. Cloning and Expression

Based on secondary structure predictions using the Profile network prediction Heidelberg (Rost and Sander, 1993) (Figure 8), four Paip1 constructs were generated for expression as hexahistidine fusion proteins. Paip1(FL), Paip1(154-375), Paip1(157-375) and Paip1(154-479) were amplified by PCR using the primers described above and subcloned into the BamH1 and EcoRI restriction sites of the bacterial expression vector pProEX-HTb (Invitrogen). Positive clones where confirmed by sequencing.

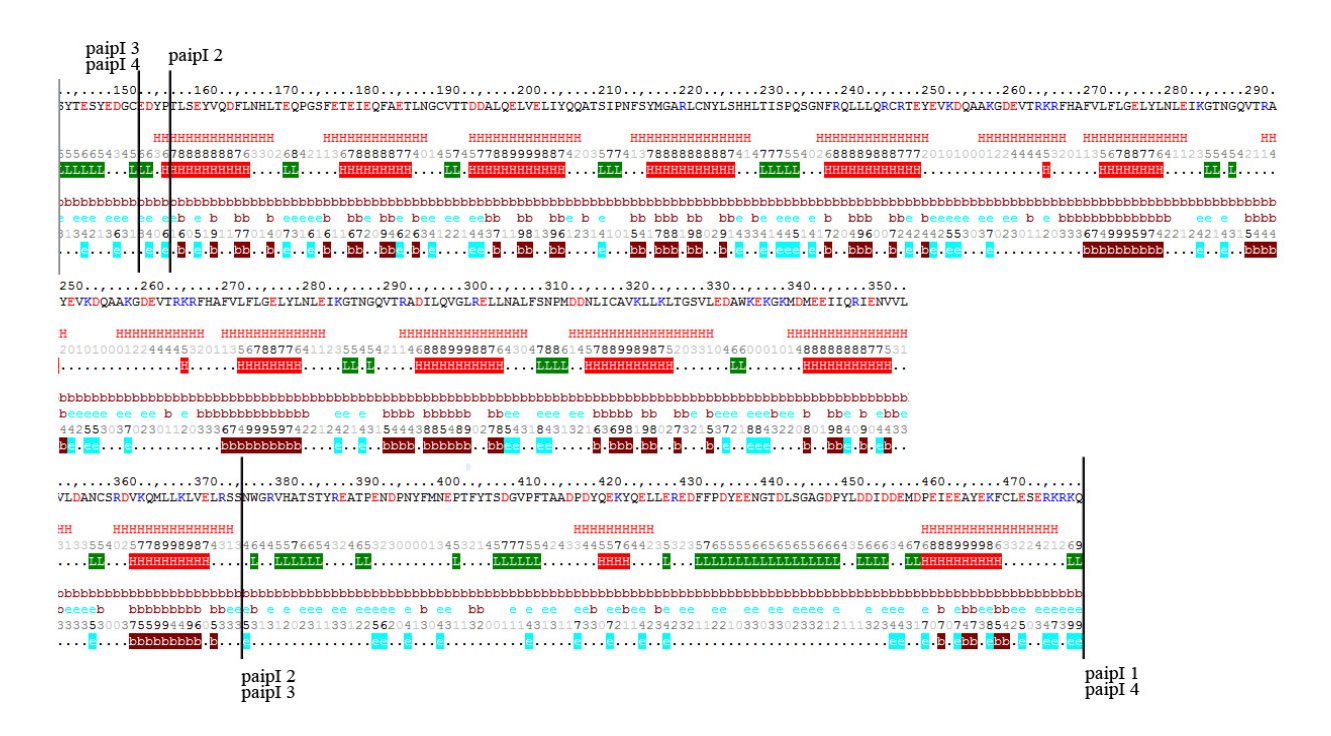


Figure 8 PROF Prediction of the secondary structure of Paip1 (143-479).

PROF analysis was used to create the four construct targets for crystallization. Paip1/1 (residues 1-479) is the full length protein, encompassing the flexible C- and N- terminal linkers. Paip1/2 (residues 157-375) includes the MIF4G domain which has been implicated in the binding of eIF3 and eIF4A. The construct terminates before the flexible C-terminal linker domains, which are unstructured regions that may affect crystallization. Paip1/3 (residues 154-375), is similar to construct 2. However, it additionally includes 3 amino acids at the N-terminus. This construct was designed since PROF analysis shows that these residues are part of a loop structure that initiates before the first helix and may affect crystallization. Paip1/4 (residues 154-375) contains all the helical domains which house the MIF4G domain, and also includes the C-terminal flexible linker region containing the PAM1 domain. PROF: H=helix, E=extended (sheet), blank=other (loop).

The generated sequences contained hexahistidine affinity tags attached at the N-termini of each recombinant protein. The affinity tags are used to facilitate purification via the workflow described below. The recombinant plasmids were then transformed into E. coli BL21(DE3) for inducible expression of the hexahistidine tagged fusion proteins. Production of recombinant proteins, tested under different expression conditions and visualized by SDS-PAGE of cell lysates, showed that all proteins expressed were soluble.

## 3.2. Purification of Paip1 constructs and eIF4A

Cell lysates of 4 liters of bacterial culture of Paip1(FL), Paip1(154-375), Paip1(157-375) and Paip1(154-479) contained in 25mM Tris (pH8.0), 500mM NaCl, 5% glycerol and 10mM imidazole (NiA buffer), were loaded onto a Ni-NTA affinity column (HisTrap FF Columns, GE healthcare) equilibrated with NiA buffer and eluted using a linear gradient with increasing imidazole. The elution buffer contained 25mM Tris-HCl pH 8.0, 500 mM NaCl, 500mM imidazole and 5% glycerol (NiB Buffer). An automated program controlled by the ÄKTA purifier system (GE Healthcare Life Sciences) was utilized to vary the imidazole concentration between 10 mM and 500 mM. Figure 9 depicts the UV<sub>280nm</sub> absorbance for Paip1(157-375) — henceforth referred to as MPaip1 — during loading onto and elution off the Ni affinity column. A single peak occurred during elution which was characterized on an SDS-PAGE gel (25kDA) shown in the inset of figure 9.

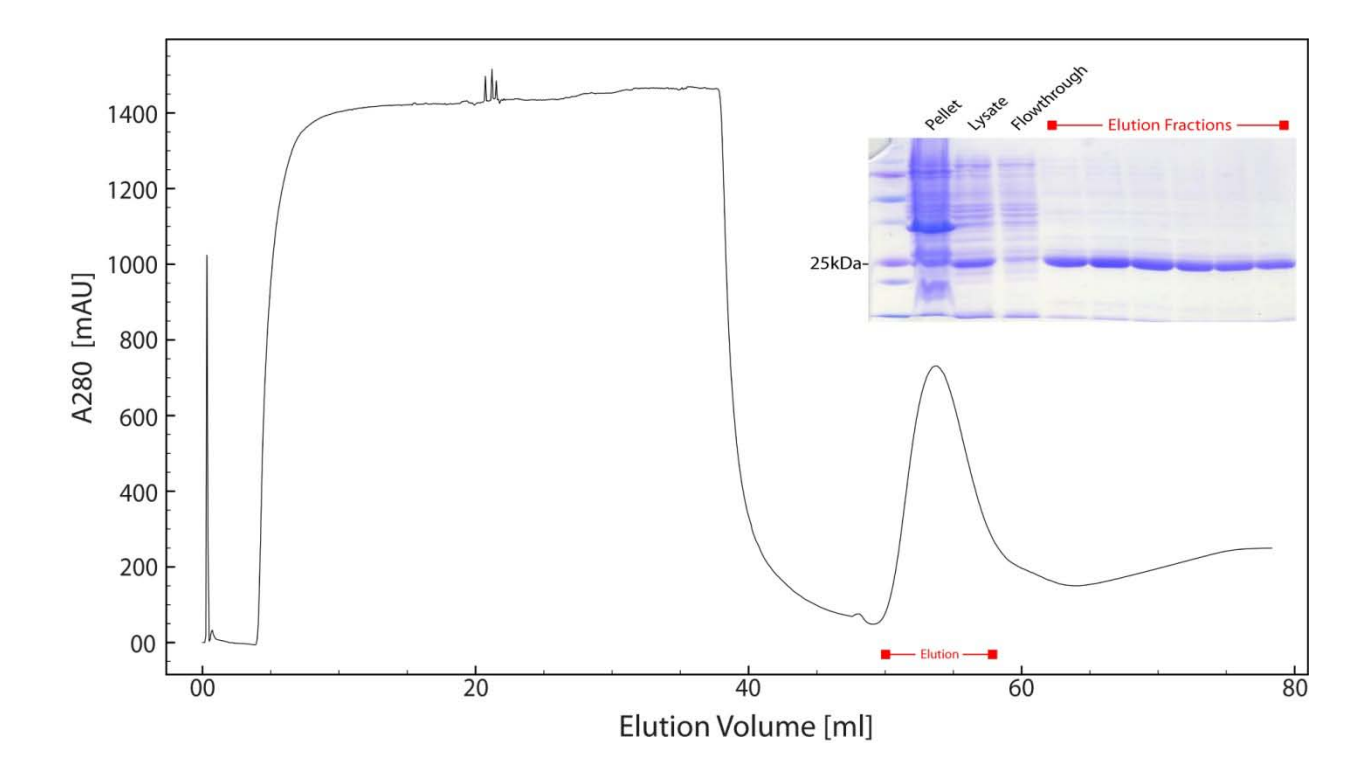


Figure 9 Chromatogram and SDS-PAGE (inset) of the Ni affinity purification step of MPaip1. The region outlined by the red line indicates the fractions that have been identified by SDS-PAGE. The inset shows the coomassie stained SDS-PAGE gel (12%) of the molecular marker (lane 1) the Pellet (lane 2), soluble protein (lane 3) flow-through (lane 4) and the collected fractions of the Ni affinity column (lanes 5-10).

The eluted fractions of MPaip1 were then pooled and dialyzed overnight against a buffer containing 25mM Tris (pH8.0), 500mM NaCl, 5% glycerol and tobacco etch virus (TEV) protease (1mg protease per app. 25 mg protein) for the cleave of the N-terminal hexahistidine tags. The sample was then purified thorough a second bout of Ni-NTA affinity to clear the sample from the cleaved hexahistidine tags and other impurities. A molecular weight shift due to TEV protease digestion was observed (Figure 10 inset, lanes 2 and 3). The eluate was concentrated to a volume of 5 ml and diluted 10x with a buffer containing 25mM Tris-HCl pH 8.0 and 5% glycerol (QD buffer); thus preparing it for a purification step based on surface charge using an anion exchange chromatography column (HiTrap chelating HP,GE healthcare). Once the sample was loaded onto the HiTrap column equilibrated with a buffer containing 25mM Tris-HCl pH 8.0, 50mM NaCl and 5% glycerol (QA buffer), a linear gradient was used to elute the

sample by increasing the salt concentration of the buffer to 500 mM NaCl (QB buffer). A single peak occurred during elution generating a highly homogenous and pure MPaip1 protein sample as characterized by the chromatogram and SDS-PAGE (Figure 10).

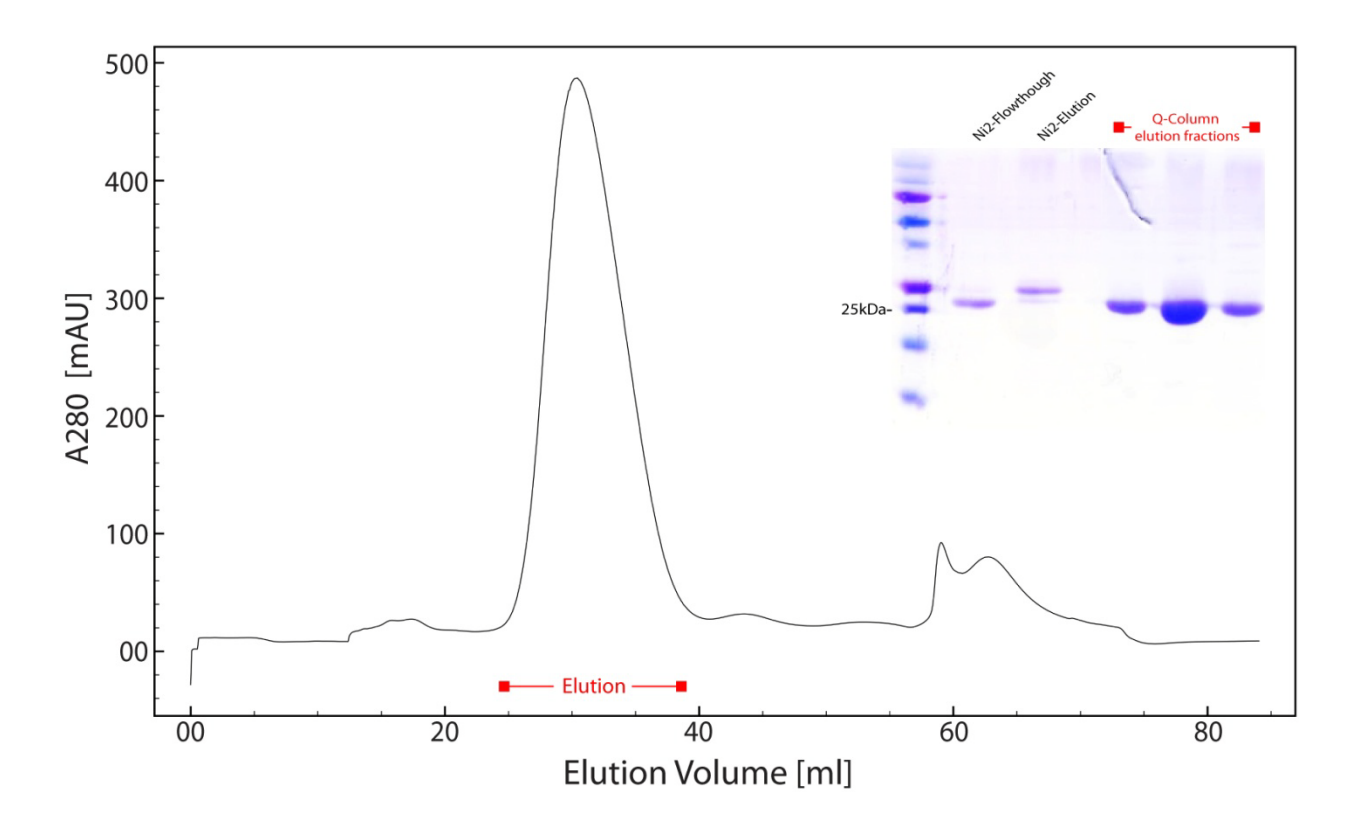


Figure 10 Chromatogram and SDS-PAGE(inset) of the anion exchange purification step of MPaip1. The region outlined by the red line indicates the fractions that have been identified by SDS-PAGE. The inset shows the coomasie stained SDS-PAGE gel (12%) of the molecular marker (lane 1); the flow-through (lane 2) and elution (lane 3) of the Ni-affinity purification step; and the pooled fractions following anion exchange chromatography elution (lanes 4-6). The molecular weight shift observed between the flow-through and elution of the Ni-affinity purification step indicates that the hexahistidine tags have been successfully digested via the overnight cleavage with TEV protease.

To further dispose of impurities in the protein sample; to determine the apparent molecular weight; and to analyze the polydispersity of the protein in solution, size exclusion chromatography (gel filtration analysis) was performed. MPaip1 fractions were pooled and concentrated to a final volume of 500 µl and injected into a 24ml Superdex<sup>™</sup> 75 gel filtration column (10/300, GE Healthcare) equilibrated in a 25 mM Tris-HCl pH 8.0, 200 mM NaCl and 5% glycerol buffer (GF buffer). Gel filtration analysis

resulted in single symmetric peak centered around a retention volume that indicated that MPaip1 is a monomer (Figure 11). SDS-PAGE indicated the protein was greater than 95% pure (Figure 11, inset).

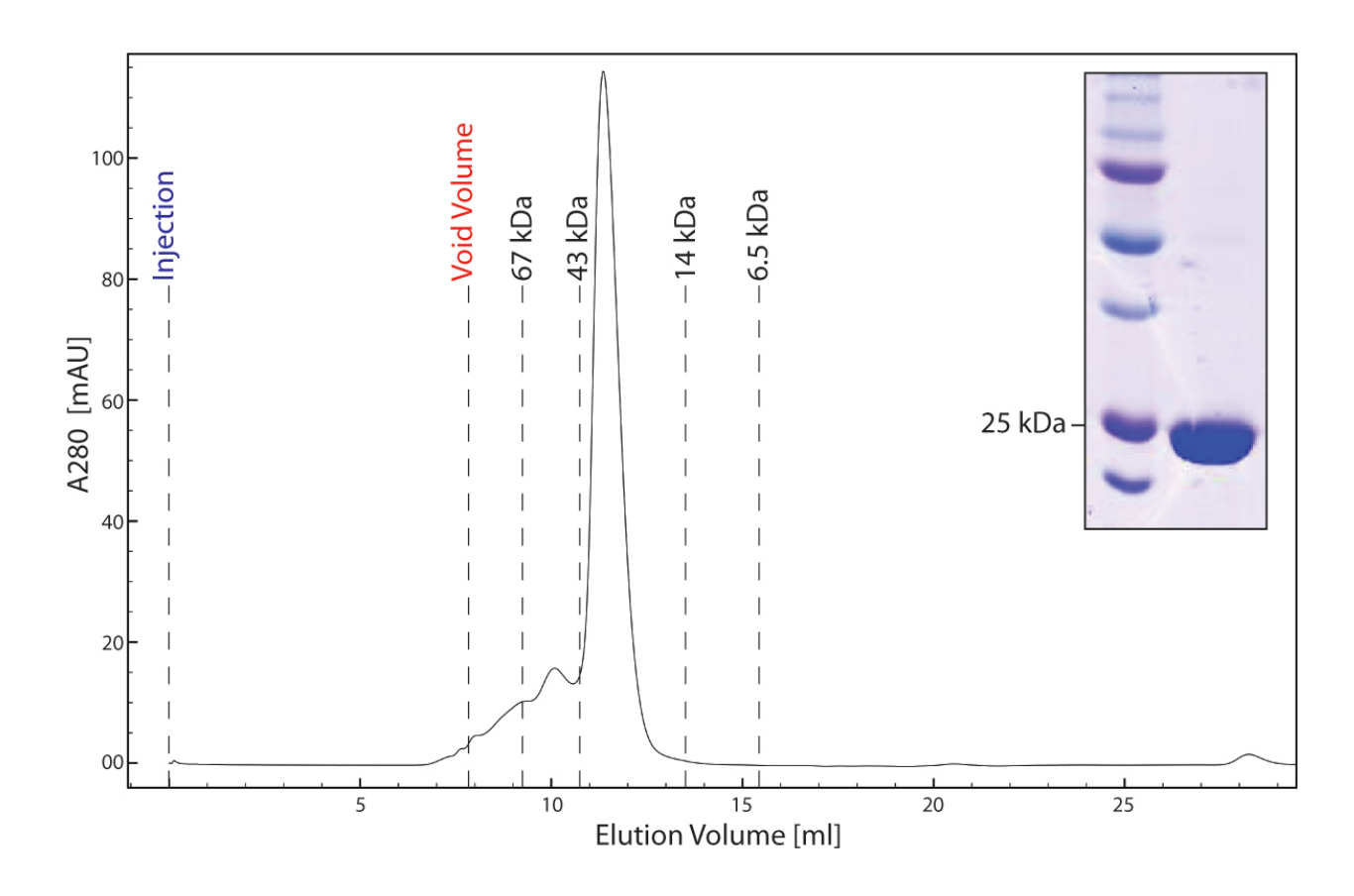


Figure 11 Chromatogram of analytical gel filtration and SDS-PAGE analysis (inset) of purified MPaip1.

Gel filtration was carried out on a 24 mL S75 column (GE) which has a cut-off of 70 kDa and a void volume of ~8 mL. Vertical lines indicate the positions of molecular weight standards. The shoulder to the left of the main peak indicates higher molecular weight species that were omitted from the final pool. SDS-PAGE was carried out on a 12% polyacrylamide gel and the bands were visualized by Coomassie staining. Lane 1 contains molecular-weight markers and lane 2 contains the purified recombinant MPaip1 protein.

Purified Mpaip1 protein was either frozen in liquid nitrogen and stored at -80°C; or concentrated to 15 and 25mg/ml for crystallization experiment. Purity is an essential factor in protein crystallization and a drastic improvement in the purity of the proteins can be observed on the gels after each purification step. Electrospray mass spectrometry revealed a mass of 25366 Da which agrees well with the calculated mass

of 25368 Da for the amino acid sequence (Figure 15a). The same overall purification procedure was followed for Paip1(FT), Paip1(154-375) and Paip1(154-479) and eIF4A; which exhibited single peaks during elution's of the Ni affinity, anion exchange and gel-filtration columns. SDS-PAGE bands were visible around the expected molecular weights of 54kDa, 25kDa and 30kDa and 45 kDa for Paip1, Paip1(154-375) and Paip1(154-479) and eIF4A, respectively (data not shown).

#### 3.3. Crystallization of MPaip1

Purified preparations of MPaip1 yielded diffraction quality crystals (Figure 12), while Paip1(FT), Paip1(154-375), Paip1(154-479) failed to crystallize probably due to the unstructured regions at the N- and C- termini as suggested by secondary structure predictions. Of the ~500 different crystallization conditions tested, three conditions produced what appeared to be protein crystals. MPaip1 crystals were obtained using sitting drop vapour diffusion, against reservoirs containing (a) 0.2 M CaCl2, 20%(wt/vol) PEG 3350, (b) 0.1 M MES pH 6.5, 15% PEG20,000 and (c) 0.1M CH3COONH4, 0.1 M Bis-Tris pH 5.5, 17% PEG 10,000 at 295K. Condition (b) gave the best crystals which were reproduced via the hanging drop diffusion on 24 well plates using solutions prepared in-house. The conditions under which the best diffraction quality crystals appeared were further optimized by changing the concentrations of the protein, precipitant and salt; and by changing the pH of the buffer. The condition composed of 0.1 M MES pH 6.5, 22% PEG20K produced the best crystals which diffracted to a good resolution in early diffraction screens (Figure 13). In all cases, the crystals grew as fused clusters and had to be manually pried apart for data collection.

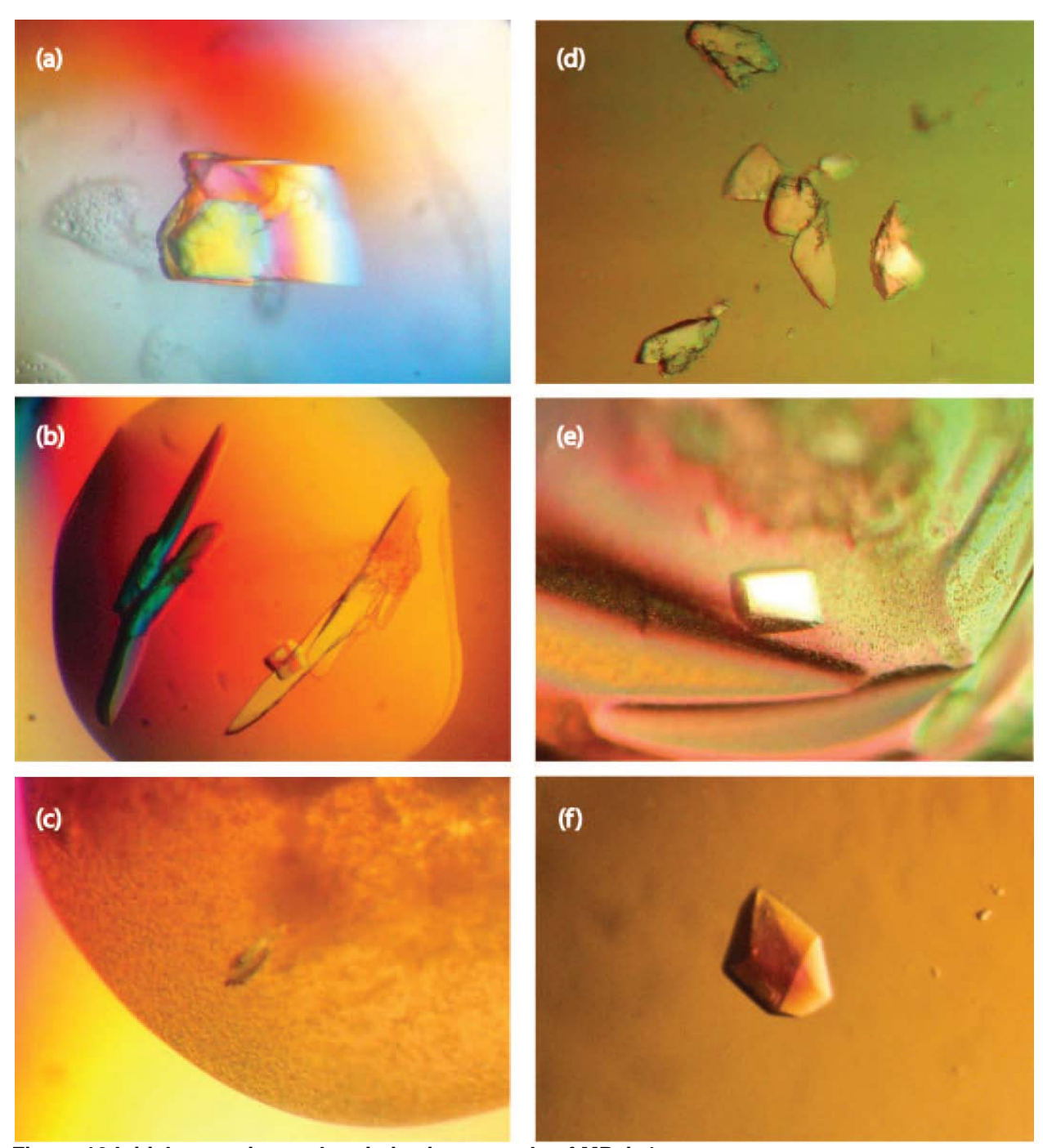


Figure 12 Initial screening and optimization crystals of MPaip1.

Protein crystallization was conducted at concentrations 25 mg/ml of MPaip1 at room temperature (295 K). Classics I, Classics II, Sparse Matrix I, Sparse Matrix II and PEG-ion (Qiagen) screens were set up using the sitting-drop vapour diffusion method (100 nL of protein solution mixed with 100 nL of crystallization condition) on Intelli-Plate™ 96x2 well plates utilizing a Phoenix Crystallization Robot (Art Robbins). The drops were sealed with clear seal tape and allowed to equilibrate against 100 μL of reservoir solution. Conditions (a) 0.2 M CaCl₂, 20%(wt/vol) PEG 3350, (b) 0.1 M MES pH 6.5, 15% PEG20,000 and (c) 0.1M CH3COONH4, 0.1 M Bis-Tris pH 5.5, 17% PEG 10,000 at 295K generated crystals after 48 hours. The three condition were then tested for reproducibility with Condition (b) giving the best crystals which were reproduced after 24 hours via the hanging drop diffusion method on 24 well plates using solutions prepared in-house. Condition (b) was further optimized by changing the concentrations of the protein, precipitant and salt; and by changing the pH of the buffer. Conditions (d), (e) and (f) had a slight variability in the concentration of PEG (10%, 21% and 22% respectively) and produced the best crystals which diffracted to a 2.5Å in early diffraction screens.

#### 3.4. Diffraction screening and molecular replacement

MPaip1 crystals belonging to condition *f* (Figure 12), which was composed of 0.1 M MES pH 6.5, 22% PEG20,000, were tested for X-ray diffraction on an in house Rigaku rotating copper-anode generator outfitted with Osmic confocal optics and an R-AXIS IV++ image-plate detector (Berghuis Laboratory). The crystals diffract X-rays to beyond 2.2 Å (Figure 13) and belong to the monoclinic space group P21.

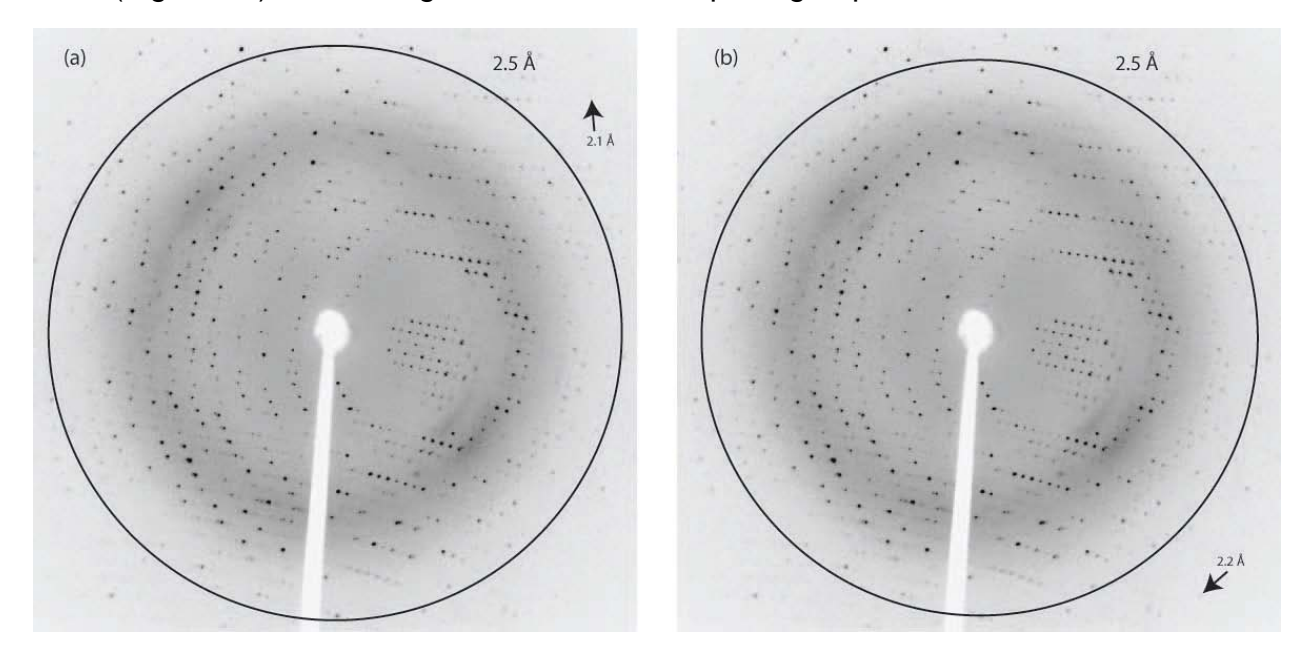


Figure 13 Representative X-ray diffraction patterns of MPaip1 obtained on a home rotating-anode source.

Black circles denote a resolution of 2.5 Å. High resolution spots are indicated with arrows. Panels (a) and (b) are approximately 90° apart in reciprocal space.

Matthews's coefficient analysis indicated that there are most likely two molecules in the asymmetric unit resulting in a solvent content of ~50%. Since this region of Paip1 has been identified as a putative MIF4G domain we attempted to solve the structure with molecular replacement using the crystal structure of the MIF4G domain of eIF4G (PDB code 1HU3; chain A) as a search model in the program PHASER (McCoy, 2007; McCoy et al., 2007). Unfortunately, this did not yield any obvious solutions. There is only 21% sequence identity between eIF4G and MPaip1, indicating that there may be significant

structural differences and that this may be a borderline case for the molecular replacement technique. Self-rotation function analysis did not reveal the presence of any non-crystallographic two-fold rotational symmetry. However, inspection of the native Patterson map reveals a 25σ non-origin peak at u=0.42, v=0.5, w=0.06, indicating the presence of translational symmetry within the unit cell (Figure 14). Thus, one possibility is that the two molecules in the asymmetric unit may be related by a pure translation. Alternatively, since the peak is on the Harker section, the two molecules may be related by a two-fold non-crystallographic rotation axis that is coincident with the crystallographic two-fold. Such a situation makes it difficult to solve a crystal structure by molecular replacement. and combined with the low sequence identity between the search model and MPaip1, experimental phases using SeMet substituted crystals can be determined using multiwavelength anomalous dispersion (MAD) or single wavelength anomalous dispersion (SAD) techniques (Hendrickson, 1991).

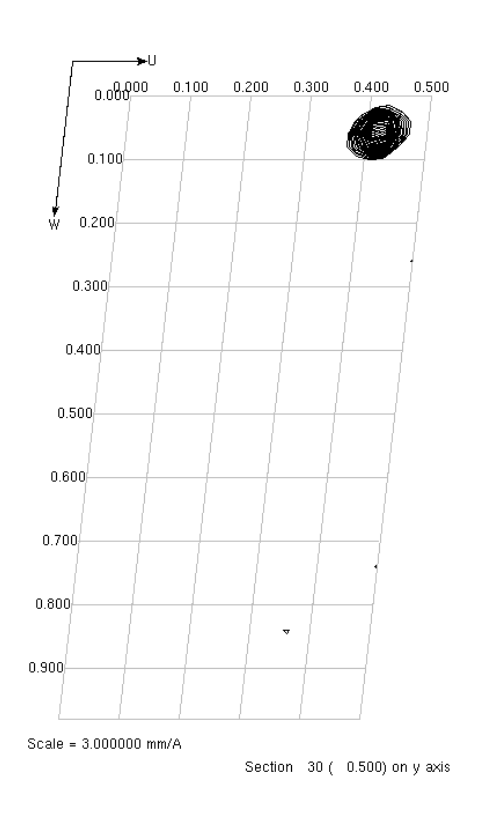


Figure 14 Harker section (v=0.5) from the native Patterson function of MPaip1 diffraction data. The map is calculated using data between 50 - 4 Å resolution and contoured beginning at  $3\sigma$  above the mean in steps of  $1\sigma$ .

#### 3.5. Expression, Purification and Mass spectrometry of SeMet MPaip1

L-SeMet labeling was performed using the methionine pathway inhibition procedure (Doublie, 1997). The same expression and purification procedures outlined above were followed for SeMet MPaip1, generating yields similar to the wild-type purification (~5 mg protein / L culture. The L-SeMet substituted protein crystallized under conditions similar to that of wild-type protein (0.1 M MES pH 6.5, 19-22% PEG20,000).

In order to investigate the incorporation of L-SeMet, electrospray mass spectrometry analysis of native and Se-Met MPaip1 was performed to accurately measure the molecular weight. Mass spectrometry showed that the Se-Met MPaip1 sample is homogenous with a molecular mass of 25648 Da, which agrees well with the calculated mass of 25649 Da (Figure 15b). Therefore, the resulting difference between native and selenomethionine labeled protein is 282.6 mass units. Given that the expected mass difference for the substitution of six Met residues with L-SeMet is expected to be ~281 Da, electrospray mass spectrometry analysis of SeMet MPaip1 indicated that there was near full incorporation of L-SeMet within the protein.

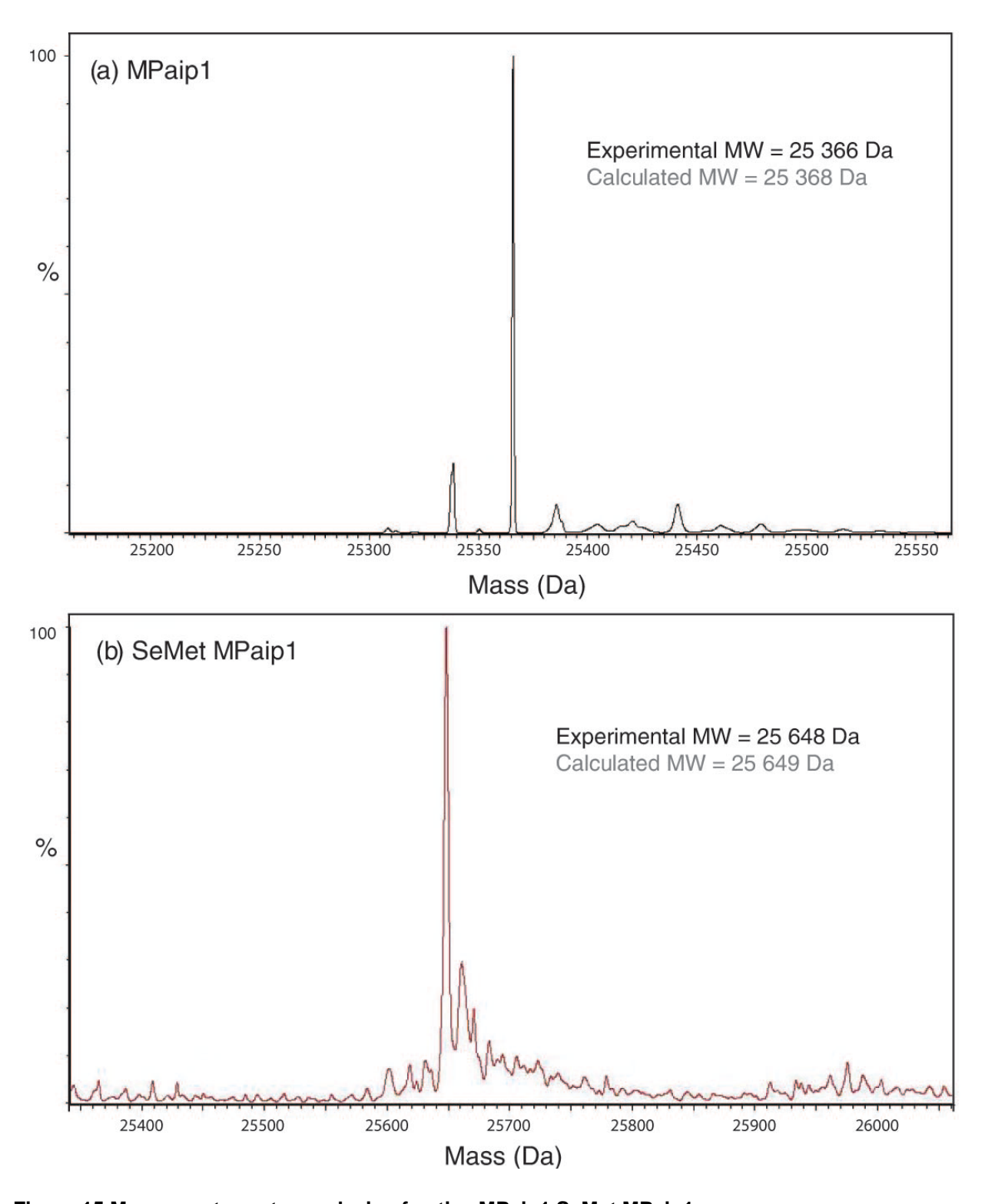


Figure 15 Mass spectrometry analysis of native MPaip1 SeMet MPaip1.

The increase in mass of the SeMet protein is due to the substitution of Met residues with SeMet.

Native protein revealed a peak at 25 366 Da while selenomethionine protein revealed a peak at 25 649 Da. The difference in values corresponds to a 281 kDa difference, which indicates that 6 L-SeMet molecules have been incorporated into the native MPaip1 sequence.

#### 3.6. Diffraction, phasing and data analysis

Both MAD and SAD data were collected at the synchrotron in Cornell (CHESS), where a tunable source of X-rays is available. The best data was collected at beamline A1 where a SAD data set diffracting to 1.8 Å was measured. The structure was solved using the peak wavelength of selenium edge. There were two molecules in the asymmetric unit and therefore 12 selenium sites were expected. The program SOLVE (Terwilliger and Berendzen, 1999) found 7 of these 12 sites which were then used to calculate initial phases that resulted in an electron density map which could not unambiguously be traced. Density modification of this map with the program RESOLVE (Terwilliger, 2000), yielded a very high quality map with an overall figure of merit of 0.57 and reliable phase information up to 1.7 Å. Refinement of the built model is currently in progress with an R-free of 26.8% and an R-factor of 25.6%. Some of the flexible loops in the structure remain to be built and waters have not been added yet. However, for the purposes of this thesis the structure is at a stage of refinement where it can be reliably interpreted.

**Table 1 Crystal parameters and data-collection statistics for MPaip1 crystals** Values in parentheses are for the outer resolution shell.

values in parentileses are for the outer resolution shell.		
Wavelength (Å)	Home-source 1.54	SAD 0.9789
Resolution (Å)	2.20	1.70
Space group	P2(1)	P2(1)
Unit-cell parameters	a=58.8, b=75.6, c= 62.0	a=58.763, b=75.641, c= 61.981
a (Å)	$\alpha$ =90.0, $\beta$ = 95.3, $\gamma$ =90.0	$\alpha$ =90.000, $\beta$ = 95.257, $\gamma$ =90.000
No. of observations	178637	334588
No. of unique reflections	25466	58807
Mosaicity (°)	1.2	0.4
$R_{merge}^{\ \ \ \ \ \ \ }$	4.7 (56.7)	6.6 (54.8)
Completeness (%)	91.0 (56.7)	99% (94.8%)
// σ( <b>/</b> )	32.3 (9.0)	19.5 (2.3)
Redundancy	7.0 (5.0)	5.7 (4.4)

<sup>#</sup>  $R_{\text{merge}}$  is defined as  $\sum_{hkl}\sum_{i}|I_{i}(hkl)-\langle I(hkl)\rangle|/\sum_{hkl}\sum_{i}I_{i}(hkl)$ , where  $I_{i}(hkl)$  is the intensity for the ith observation of a reflection with Miller indices hkl and  $\langle I(hkl)\rangle$  is the mean intensity for all measured values of I(hkl) and its Friedel pair.

#### 3.7. MPaip1 Structural overview

MPaip1 is a crescent shaped deca-helical molecule that belongs to the HEAT-repeat family of proteins. The crystal structure of MPaip1 consists of ten antiparallel  $\alpha$ -helices of varying lengths, resulting in a molecule with dimensions of 59 Å (length) x 32 Å (depth) x 38 Å (width) as schematically illustrated in Figure 16. Here I follow the designation followed by Marcotrigiano et al. for the structure of MIF4GII (PDB ID:1HU3) where the repeats are similarly stacked in the order 1a-1b-2a-2b-3a-3b-4a-4b-5a-5b (Marcotrigiano et al., 2001). The crescent shaped middle domain of Paip1 is the result of the five repeating units of antiparallel  $\alpha$ -helices, where HEAT-repeats 1 and 2; and 3,4 and 5 are stacked in parallel order to each other. The major rotation that produces the crescent occurs at Pro-233 between 2b and 3a. Apparent kinks in the structure are found in helices 1b, 3a and 4b and are not the result of the presence of any Proline resides. Three of the four Prolines found in MPaip1 are conserved (Figure 17) and all four are found in inter- and intra-loop structures at the beginning of helices 1b, 2b, 3a and 4**b**. Hydrophobic residues line the contact face of the  $\alpha$  helices resulting in noncovalent interactions that cause the stabilization of adjacent repeats that run along the sequence, thus shaping an extended hydrophobic core characteristic of higher number HEAT-repeats (Andrade and Bork, 1995). Consequently, the structure takes the shape of a right handed solenoid with a superhelical axis perpendicular to axes of the decaantiparallel  $\alpha$  helices. The orientation of the repeating **a** and **b**  $\alpha$ -helices pattern the structure in way such that it has a convex and a concave surface respectively. The a and b helices are opposed in direction and in consequence their allied loops segregate to opposite sides of crescent surface.

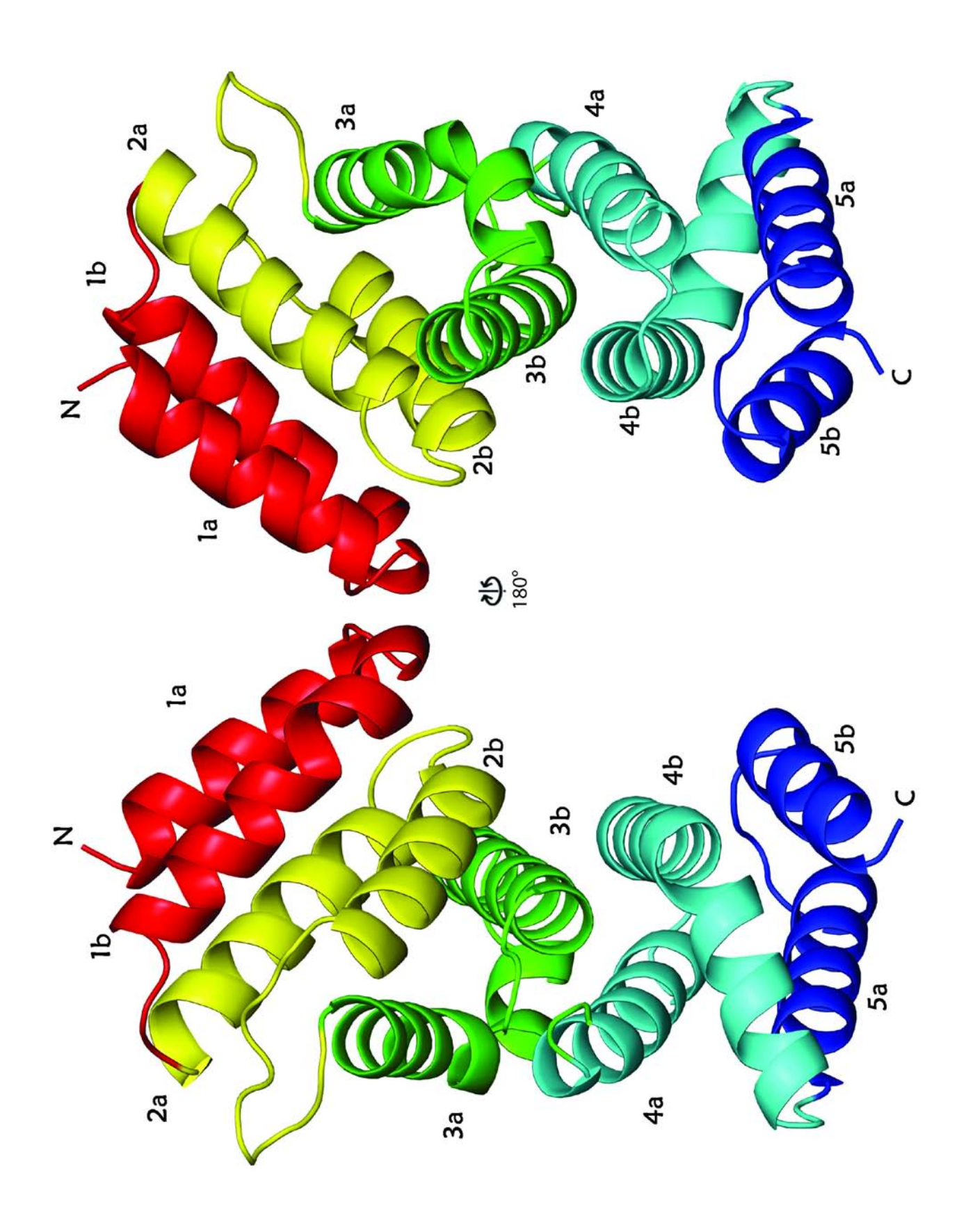


Figure 16 X-ray Crystal Structure of MPaip1 (Paip1<sub>157-375</sub>).

HEAT motifs are tandemly repeated sequences of approximately 50 amino acid, with a regular three-dimensional structure of  $\alpha$ -helical domains that pack together to form elongated solenoids (Andrade and Bork, 1995). HEAT motifs (in addition to their close relatives: ARM repeats) are among the most common tandemly repeated motifs that occur in a wide variety of eukaryotic proteins (Andrade et al., 2001; Groves and Barford, 1999; Kobe and Kajava, 2000). It has been proposed that the common phylogenetic origin of Heat-repeats are β-importins (Cingolani et al., 1999; Malik et al., 1997). The canonical HEAT-repeat consists of only two anti-parallel  $\alpha$ -helices, **a** and **b**, and two turns arranged about a common axis. These repeats are linked by flexible inter-unit loops. HEAT-repeats were initially found in a number of proteins generally involved in a diverse array of cellular processes that are dependent on the association of sizable multiprotien complexes (Andrade and Bork, 1995). The designation of HEAT-repeats originated from four primary sequences identified with the characteristic pattern: Huntington; Elongation factor 3; the PR65/A subunit of phosphatase 2A (PP2A); and the lipid kinase TOR1 (a target of rapamycin). The diversity of these proteins suggested that no shared residues have to be absolutely conserved (Andrade and Bork, 1995). A function common to many HEAT repeats is the mediation of important protein-protein interactions (Andrade and Bork, 1995). Apart from MPaip1, heat repeats are also prevalent in a number of translation related proteins that include eIF4GI, eIF4GII, DAP-5 and mTOR.

In an attempt to outline the conservation along the HEAT-repeat sequences among Paip1 species, the middle domain of Paip1 was aligned with all its known orthologs: Mus musculus (78-298); Bos taurus (78-298); Rattus norvegicus (82-302); Xenopus laevis (143-363) and Danio rerio (103-324), generating identities of 98%, 97%, 98%, 79% and 64%, respectively (Figure 17). Analysis of Multiply Aligned Sequences (AMAS) server (Barton, 1990) was used to generate conservation scores which were mapped

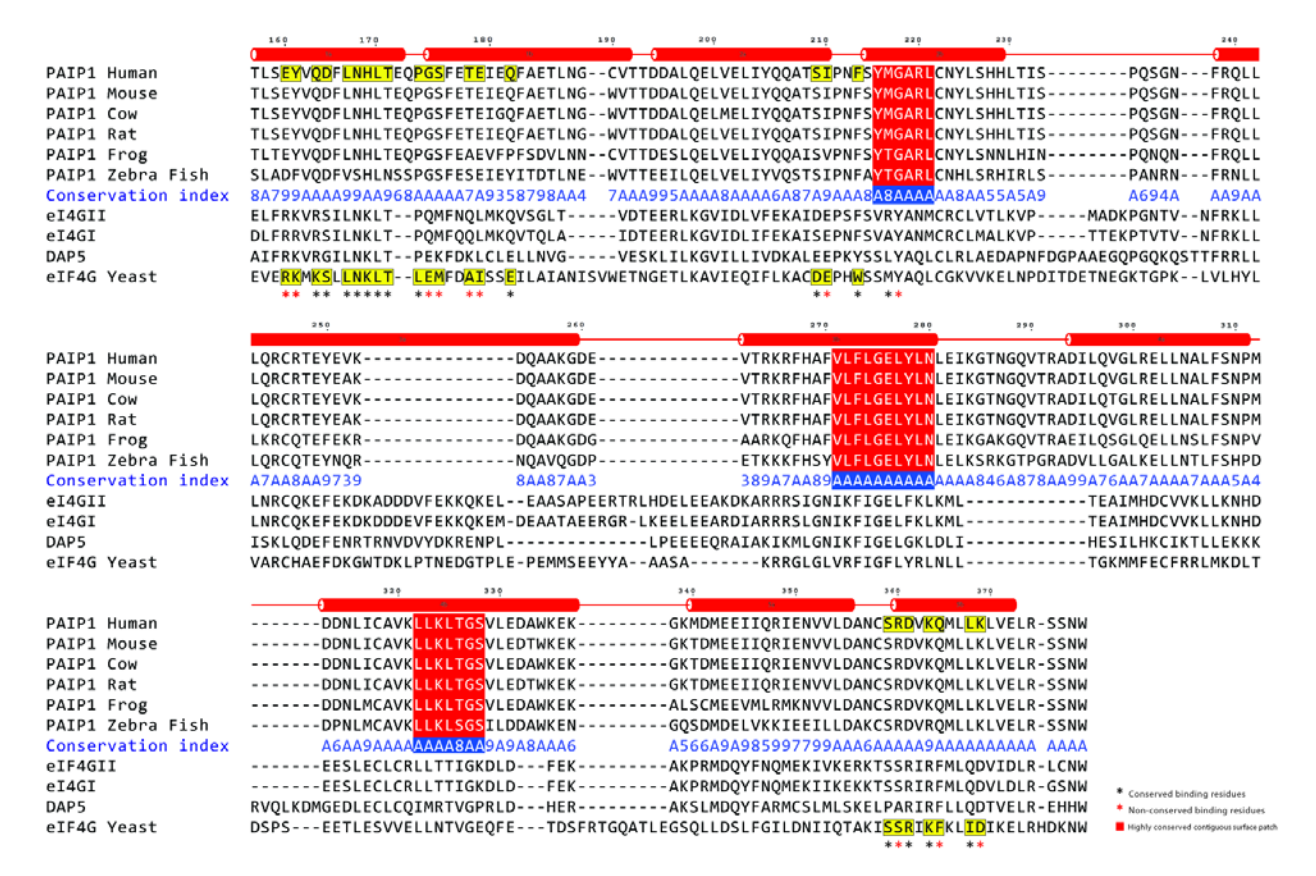


Figure 17 Multiple Sequence Alignment of several MPaip1 orthologs and homologs.

Sequence alignments of Paip1 orthologs Homo sapiens (157-371), Mus musculus (78-298, id:98%), Bos taurus (78-298, id:97%), Rattus norvegicus (82-302, id:98%), Xenopus laevis (143-363, id:79%), Danio rerio (103-324, id:64%), and Paip1 homologs elF4GII (753-984, id:26%), elF4GI (761-991, id:28%), DAP5 (76-309, id:21%) and yeast elF4GI (605-852, id:21%). AMAS server (Analysis of Multiply Aligned Sequences) was used to generate conservation scores for known Paip1 orthologs. Residues shaded in red form a contiguous surface patch outlined on the surface representation illustrations. The 27 residues corresponding to the elF4A-binding site on yeast elF4GI are shaded yellow; where a black asterisk denotes a conserved binding residue and a red asterisk denotes a non-conserved binding residue. Secondary structure elements are indicated above the alignments.

onto the surface of MPaip1 using Protskin (Deprez et al., 2005). Interestingly, the analysis generated a number of scattered yet matching sequences which formed a highly conserved contiguous patch on the surface. This highly conserved surface patch involves the helices 2**b**,3**b** and 4**b**, which are stacked on top of each other via hydrophobic interactions (Figure 18,19). Since the surface patch is both highly conserved and contiguous, it may signify functional significance of as yet unknown functions of Paip1.

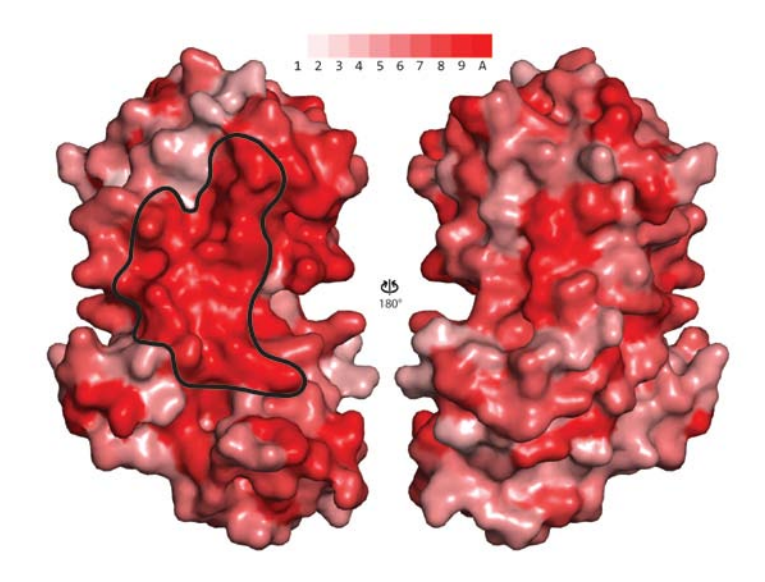


Figure 18 Surface representation of MPaip1 residues conserved among all known species.

The scores range between 1 (not conserved) and A (absolutely conserved). A highly conserved contiguous surface patch, highlighted on the left surface representation, involves the helices 2b,3b and 4b.

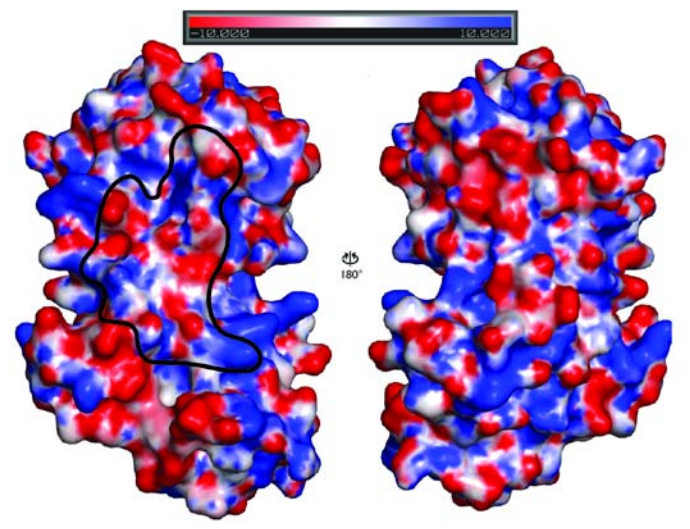


Figure 19 Electrostatic surface rendition of MPAIP1

Electrostatic potential map generated with Pymol and APBS. The surface is colour coded for calculated electrostatic potential: red (acidic) < - 10kT and blue (basic) > +10kT, where k denotes the Boltzmann Constant and T denotes temperature.

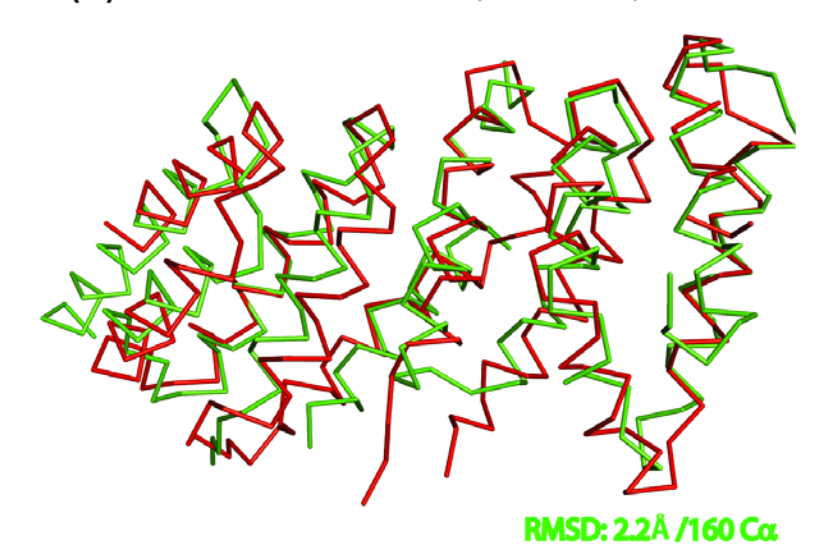
MPaip1 was also aligned with its known homologs eIF4GII (753-984), eIF4GI (761-991), DAP5 (76-309) and yeast eIF4GI (605-852) generating identities of 23%, 21%, 21% and 21% respectively (Figure 17). This information was used to map the conservation of the all known eIF4A binding sites of MIF4G onto MPaip1 (Table 2 & Figure 20).

#### 3.8. Structural and functional comparisons of MPaip1 and MIF4G

The crystal structures of two MIF4G domains; yeast eIF4GI (Schutz et al., 2008) and human eIF4GII (Marcotrigiano et al., 2001), have already been determined (Figure 21). MIF4G refers to the Middle domain of eukaryotic initiation factor 4G (eIF4G). Apart from eIF4G, MIF4G domains are found in several proteins involved in RNA metabolism; eIF-2b (translation initiation factor), UPF2 (regulator of nonsense transcripts 2) (Kadlec et al., 2004), and nuclear cap-binding proteins (CBP80, CBC1, NCBP1), (Kim et al., 2009). In general, MIF4G domains share common functions, are rich in alpha-helical HEAT-repeats and may contain multiple repeats. Nonetheless, they may differ in their sequence. (Aravind and Koonin, 2000; Ponting, 2000). In eIF4G, MIF4G is a multipurpose adaptor, which binds to the eIF4F complex, eIF4A and eIF3 (Craig et al., 1998; Imataka and Sonenberg, 1997; Lamphear et al., 1995) as well as to RNA (Pestova et al., 1996) and DNA (Kim et al., 1999).

Given the similarity between the structure and the function of the middle domains of Paip1 and eIF4G, the structures of MPaip1, eIF4GI and eIF4GII were superimposed to investigate possible correlations of their structure and function (Figure 20). The superimposition of the  $\alpha$ -carbons of MPaip1 and the  $\alpha$ -carbons of eIF4GII (PDB:1HU3) and eIF4GI (PDB:2VSO) results in root mean square deviations (RMSD) of 2.2Å and 2.8Å, respectively. Predictably, MPaip1 is closer in structure to its human MIF4GII homolog; portraying a better overlay with the eIF4A binding sites (Figure 20a). Nonetheless, MPaip1 exhibits a number of apparent differences with MIF4GII, and these include a longer 1b helix; a larger inter-helical loop between helices 3b and 4a and a bend at Lys-253 in the 3b  $\alpha$ -helix which is also longer than that of MIF4GII. In addition, MIF4GII exhibits a shorter 1a  $\alpha$ -helix. On the other hand, MPaip1 differs from MIF4GI in its 1b, 2b 3a, 4a, 4b. A Proline residue present at the origin of MPaip1s 1b  $\alpha$ -

# (a) MPAIP1/eIF4GII (PDB:1HU3)



# (b) MPAIP1/elF4GI (PDB:2VSO)

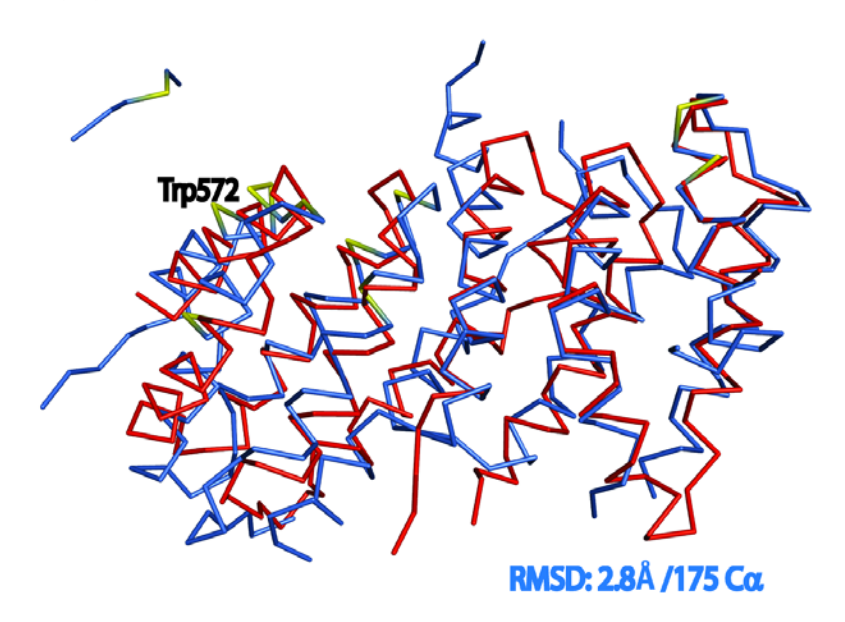


Figure 20 Overlay of MPaip1 on human and yeast MIF4G.

The superimposition of the alpha carbons of MPaip11 and the crystal structures of (a) eIF4GII (PDB:1HU3) and (b) eIF4GI (PDB:2VSO) results in root mean square deviations of 2.220Å and 2.811Å respectively.

helix results in an apparent kink at the beginning of the helix. As a result, the overlay of MPaip1s and MIF4GIs 1 $\boldsymbol{b}$   $\alpha$ -helix does not superimpose fittingly due to the absence of a Proline residue at the same juncture in MIF4GI. It is interesting to note that an eIF4A binding residue (Tyr-618) is present in MIF4GI at the same point of MPaip1s bending. Another interesting difference between MPaip1 and MIF4GI is the 3 $\boldsymbol{a}$   $\alpha$ -helix; which appears to be longer in MPaip1 due to the presence of an additional 8 residues at its C-terminal end. Moreover, MPaip1 exhibits a longer 4b helix while MIF4GI is exhibits a longer 3b helix.

Shutz et al. determined the structure of eIF4GI complex with eIF4A outlining three structurally segregated interaction surfaces on MIF4G as illustrated by the yellow residues outlined in Figure 20b and the magenta residues outlined in Figure 21c (Schutz et al., 2008). First, a significant tryptophan residue (W572) was demonstrated to be critical in the binding of eIF4A. Shortening of the eIF4G sequence at the N-terminal resulted in significant loss of binding affinity (Schutz et al., 2008). This result was also confirmed via site-directed mutagenesis and pull-down experiments. Paip1 is lacking in this key tryptophan residue, and structure based sequence alignments between the crystallized yeast eIF4GI (TIF4631) and Paip1 show that latter holds an asparagine instead. The absence of the tryptophan residue from Paip1 is thought to confer the low binding affinity between Paip1 and eIF4A as demonstrated by pull-down experiments (Figure 23).

The two other interaction surfaces on MIF4G involve its N-terminal and C-terminal, which interact with the C-terminal and N-terminal domains of eIF4A, respectively (Figure 21c). Overall, the interface between MIF4G and eIF4A contains 23 hydrogen bonds and 14 salt bridges.

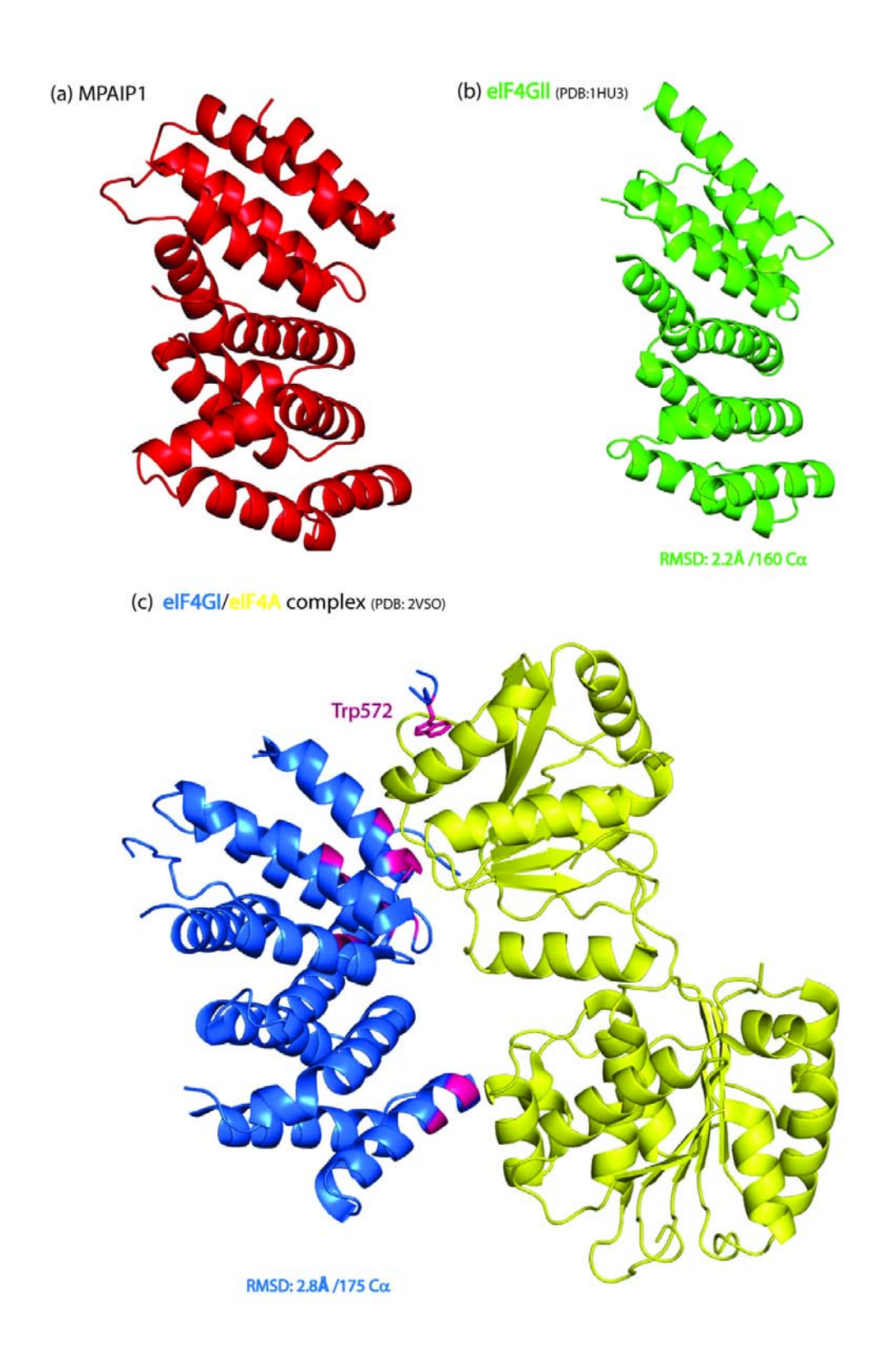


Figure 21 Crystal structures of MPaip1, MIF4GI and MIF4GII
The superposition of the alpha carbons of MPAIP1 and the crystal structures of eIF4GII (PDB:1HU3) and eIF4GI (PDB:2VSO) results in root mean square deviations of 2.220Å and 2.811Å respectively.

In an attempt to outline the possible eIF4A binding sites on MPaip1, the Protein-Protein interface analysis (PROTORP) server (Reynolds et al., 2009) was used to a analyze the interface of the yeast eIF4A/MIF4G complex. The analysis indicated that there are 34 buried residues, with the first five being upstream to the sequence of MPaip1. Employing a structure based sequence alignment approach of MPaip1 and MIF4G (PDB id: 2VSO, Chain e), the suspected eIF4A binding residues of MPaip1 were scored using the AMAS server generating conservation indices between 1 and 10(A) (Barton, 1990). The scores as well as the implicated residues are outlined in table 2. Overall, the analysis indicates that of the 34 buried residues, 8 residues are identical, 11 are similar, 10 are non-conserved and 5 are upstream to the MPaip1 sequence. The conserved MPaip1 residues that potentially bind eIF4A were then plotted on the surface of MPaip1 as illustrated in Figure 22. Interestingly, these residues do not coincide with the highly conserved surface patch en masse, indicating the conserved surface patch may confer some other as yet unknown function.

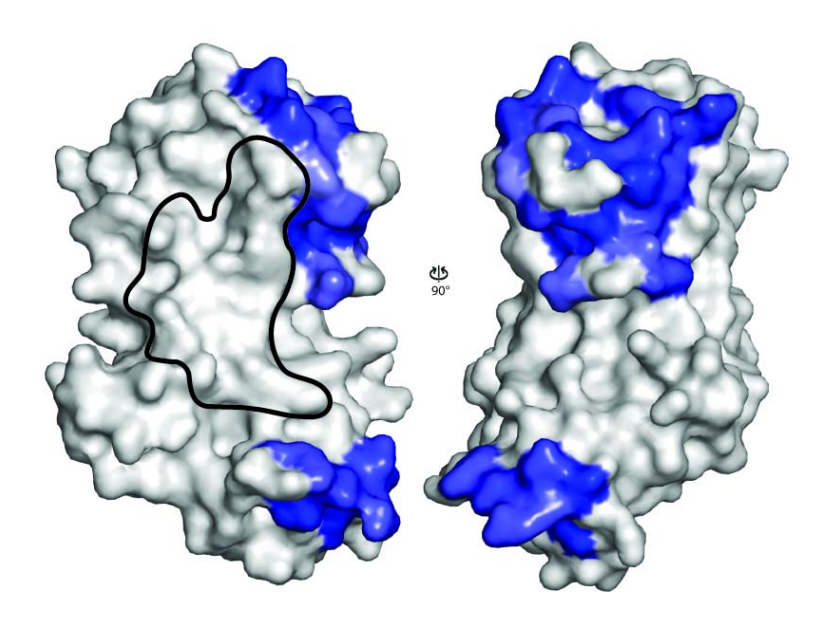


Figure 22 Surface representation of elF4A conserved binding sites on MPAIP1. The two separate blue regions denote residues involved in the elF4G-elF4A interaction (PDB 2VSO). These residues for the most part do not coincide with the highly conserved surface patch (denoted with a black lasso). The crucial elF4A binding residue Trp-579 in elF4G is lacking in the Paip1 sequence. The corresponding residue in the Paip1 sequence is an Asn residue. This could account for the weak binding affinity observed in the pulldown assays.

Table 2 List of the eIF4A binding sites of yeast MIF4GI (TIF4631) generated by the PROTROP server and their conservation indices with MPaip1 Conservation indices were generated using the AMAS server.

elF4GI	MPaip1	Conservation index
577N	-	-
578R	-	-
579W	-	-
581P	-	-
582K	-	-
608R	160E	8
609K	161Y	7
611K	163Q	7
612S	164D	7
614L	166L	10
615N	167N	10
616K	168H	9
617L	169L	10
618T	170T	10
619L	173P	6
620E	174G	4
621M	175S	6
624A	178T	8
6251	179E	5
628E	182Q	8
655K	207Q	7
658D	210S	7
659E	2111	5
661H	213N	5
662W	214F	9
665M	217M	10
666Y	218G	6
833S	<b>359S</b>	10
834S	360R	6
835R	361D	7
837K	363K	10
838F	364Q	7
841I	367L	10
842D	368K	6

#### 3.9. Binding studies

As discussed above, MIF4G and MPaip1 share homology in structure and function. Both exhibit a crescent shaped deca-helical molecule that belongs to the HEAT-repeat family of proteins and both bind eIF4A and eIF3. Here, the investigation of the MPaip1 and eIF4A binding via three biophysical methods is discussed.

His-tag pull-down experiments employing eIF4A as the bait protein were performed to analyze the binding of MPaip1 and full-length Paip1. Initially, non-specific background binding problems were encountered. This difficulty was circumvented via the use of higher imidazole wash buffer. Several experiments were run to pinpoint the buffer that resulted in optimal binding of the bait proteins and least background binding of the prey protein. At first, 0.5 mg of prey protein (His-eIF4A and eIF4G-His) were bound to a Ni-NTA-Sepharose resin acquired from HisTrap FF Column (GE healthcare) and incubated for 1 hour. Unbound protein was then washed off with a buffer containing 500mM NaCl, 25mM Tris-HCl pH 8.0, 50mM imidazole and 5% glycerol. 1 mg of bait proteins Paip1 wt, MPaip1 (157-375) and Paip1 (154-375) were then added to react with His-eIF4A and incubated for 1 hour. Additionally, 1 mg of bait protein eIF4A was added to bead bound eIF4G-His and incubated for one hour. This reaction served as a positive control, in order to confirm that the basic conditions of the experiment were able to produce a positive result. Finally, all proteins were eluted using Buffer NiB.

The results of the pull-down experiments, illustrated by the SDS-PAGE in Figure 23, show that MPaip1 and Paip1 (154-375) are unable to bind eIF4A while Paip1 binds weakly. The binding of full-length Paip1 to eIF4A was originally described by Craig et al., however, here I show that the interaction is very weak relative to eIF4G (Craig et al., 1998). This fact may be attributed to the absence of the critical tryptophan residue in MPaip1 which has been shown to be critical for eIF4A binding (Schutz et al., 2008). Sequence alignments show that the MPaip1 contains an asparagine residue instead of

the critical tryptophan residue. Accordingly, this result suggests that unlike MIF4G, the interaction of MPaip1 with eIF4A may require residues that are external to the MPaip1 sequence.

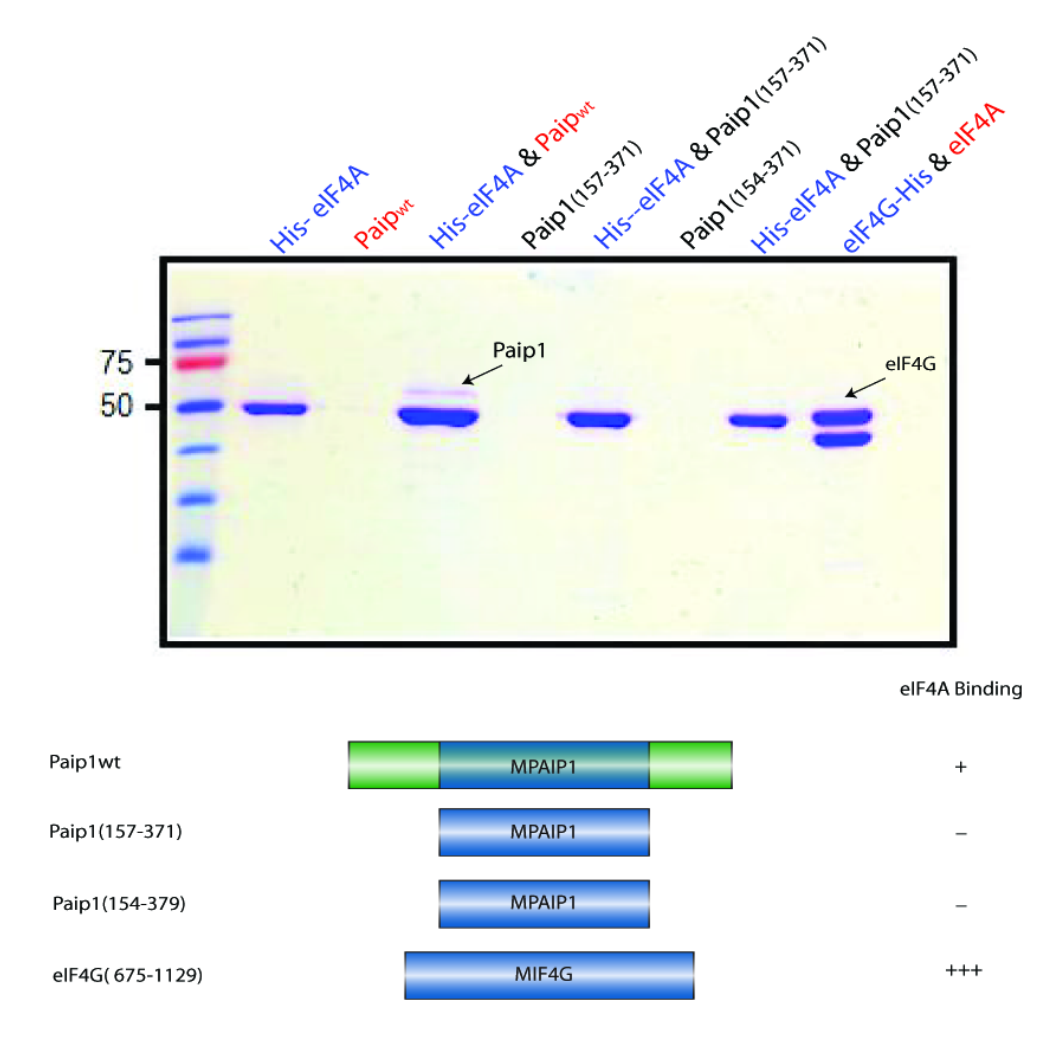


**Figure 23 SDS-PAGE analysis of Paip1, MPaip1 and elF4A pull-down experiments.**As indicated by the arrows, MPaip1 and Paip1(157-375) do not bind elF4A, while Paip1 and elF4G bind elF4A with varying degrees as illustrated by the strength of the SDS-PAGE bands.

ITC and SPR experiments were also used to investigate the interaction of MPaip1 and Paip1 with eIF4A. For the ITC experiment, MPaip1 showed no binding while Paip1 continued to aggregate in both the vessel and the syringe at various concentrations with the use of a variety of reducing agents. As a result, no dissociation data were obtained for Paip1. In addition, several trials at measuring the affinity of the Paip1 and eIF4A interaction using SPR failed.

#### 3.10. Small angle X-ray Scattering (SAXS) analysis of MPaip1

In order to obtain a picture of the overall configuration of the MPaip1 directly in solution, Small Angle X-ray Scattering (SAXS) analysis was employed. SAXS is an analytical method used to determine the structure of a particle system in terms of averaged particle systems of shapes at low resolution. It is used on non-crystalline material, such as proteins in solution and can also be applied to study the structure of DNA, viruses and polymers. Due to the random orientation of the molecules in solution and the lack of regularity typically seen in solid crystals, only low resolution structural information can be obtained using SAXS. In a typical set-up, the structure size that can be resolved ranges from 1 to 50 nm. SAXS is based on the irradiation of a sample by a monochromatic X-ray beam followed by the collection of diffraction data at very low scattering angles, typically between 0.1°-10°. As a result, the intensity distribution of the scattered beam at these low angles provides structural information about the protein sample in question. Due to the disorder of proteins in solution, averaging occurs and leads to a loss of information. Thus, SAXS does not provide high resolution information but could be useful to obtain information for the size and shape of a particle in solution. The ability to study a particle in solution in order to obtain a low resolution envelope structure is a main advantage SAXS has over X-ray crystallography. Another advantage is the requirement of less material to carry out SAXS. Additionally, in some cases SAXS is used over NMR since there are no size restrictions on the particle in question.

The aim of this experiment is to assess the structure of MPaip1 directly in solution and to use the crystal structure determined in this thesis to confirm the validity of using SAXS on this protein. Once this is established, the SAXS technique can then be used to study larger constructs of Paip1 for which crystal structures are not available. In particular, constructs of Paip1 encompassing the flexible binding regions PAM1 and PAM2 regions can be studied in complex with PABP. SAXS analysis of MPaip1 was

conducted at a concentration of 5 mg/ml in a buffer containing 50 mM Tris-HCl pH 8.0, 150 mM NaCl, 5% glycerol and 1mmDTT. Figure 24 illustrates the primary scattering data where the scattered intensity is plotted as function of scattering angle. The data were collected up to a resolution of 0.3 Å<sup>-1</sup>, which corresponds to approximately a 20 Å resolution. The fall-off in intensity with increasing scattering angle is characteristic of the overall shape of the protein and therefore can be used to determine shape information at low resolution. Guinier analysis of scattering data allows for the determination of the radius of gyration  $R_{\rm g}$  of an arbitrarily shaped particle (Sorensen and Shi, 2000). The Guinier formula is based on a second-order expansion of the structure factor of the particle; which is the square of the Fourier transform of the density distribution of the particle (Sorensen and Shi, 2000). Guinier analysis of the data resulted in a 28.3 Å radius of gyration (Figure 24). However, the  $R_{\rm g}$  derived from the crystal structure is close to 21 Å. The divergence between the experimental and the calculated radii of gyration may be attributed to the equilibrium generated between dimers and monomers present in the solution. In other words, the presence of a small fraction of dimers is skewing the Rg to a larger value than if only monomers were present. Typically, shape reconstruction using SAXS in such situations is difficult since the scattered intensity contains an average of both monomers and dimers. However, since gel-filtration analysis had previously revealed that the majority of MPaip1 molecules exist as monomers in solution (Figure 11), shape reconstruction was attempted. Fourier transformation of the primary scattering data using the program GNOM (Svergun, 1991, 1992) results in the distance distribution function which is a plot of the frequency of observed interatomic distances present within the molecule. The parameters that can be extracted from this function are the maximum dimension (Dmax) of the scattering particle and another assessment of the Rg using all of the data instead of only the low resolution data as in Guinier analysis. The distance distribution function indicated that the D<sub>max</sub> is 90 Å. This value is substantially larger than the maximum dimension of the crystal structure of MPaip1 which is approximately 60 Å. Again, this

disparity may also be due to the presence of dimers in solution, which cause the curve to be skewed (Figure 24). The Rg obtained from the distance distribution function was 28.2 Å, in good agreement with that obtained from Guinier analysis. A shape construction using the program GASBOR (Svergun et al., 2001) was then attempted. GASBOR utilizes an *ab initio* method for building structural models of proteins from SAXS data. The program uses simulated annealing in order to find a chain-compatible spatial distribution of dummy residues which fit the experimental SAXS scattering to a resolution of up to 0.5 A<sup>-1</sup> (Svergun et al., 2001).

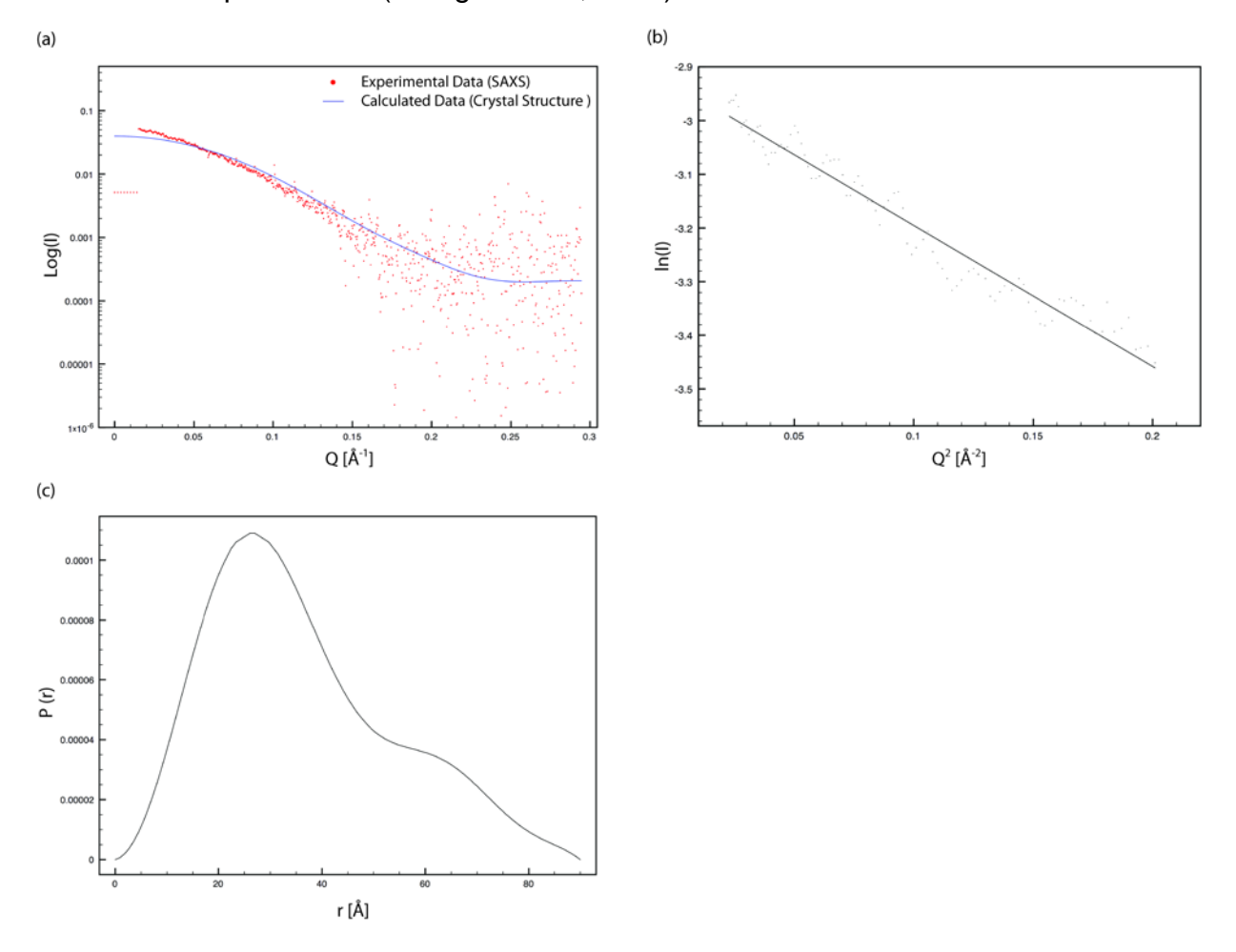


Figure 24 SAXS results for MPaip1

(a) The primary scattering data for MPaip1 showing SAXS experimental data (red dots) and the crystal structure calculated data (blue line). (b) Guinier analysis plot which generated a 28.3 Å radius of gyration (c) The plot of distance distribution function which generated a dmax 90 Å. The value is relatively larger the maximum dimension obtained from the crystal structure (~60 Å). This disparity is likely due to the presence of some dimers in the solution which apparently skew the curve.

Ten independent runs of the program GASBOR were executed and the resulting shapes were superimposed, averaged and filtered to a volume expected to be occupied by a monomer. The overall shape of the SAXS model agrees fairly well with the crystal structure of MPaip1 (Figure 25). The SAXS model, however, exhibits a region of extra volume on the concave side of MPaip1, and this is probably due to the presence of minor dimer fraction. This information is a good starting point for SAXS analysis of larger constructs of Paip1 which failed to crystallize due to the presence of flexible regions.

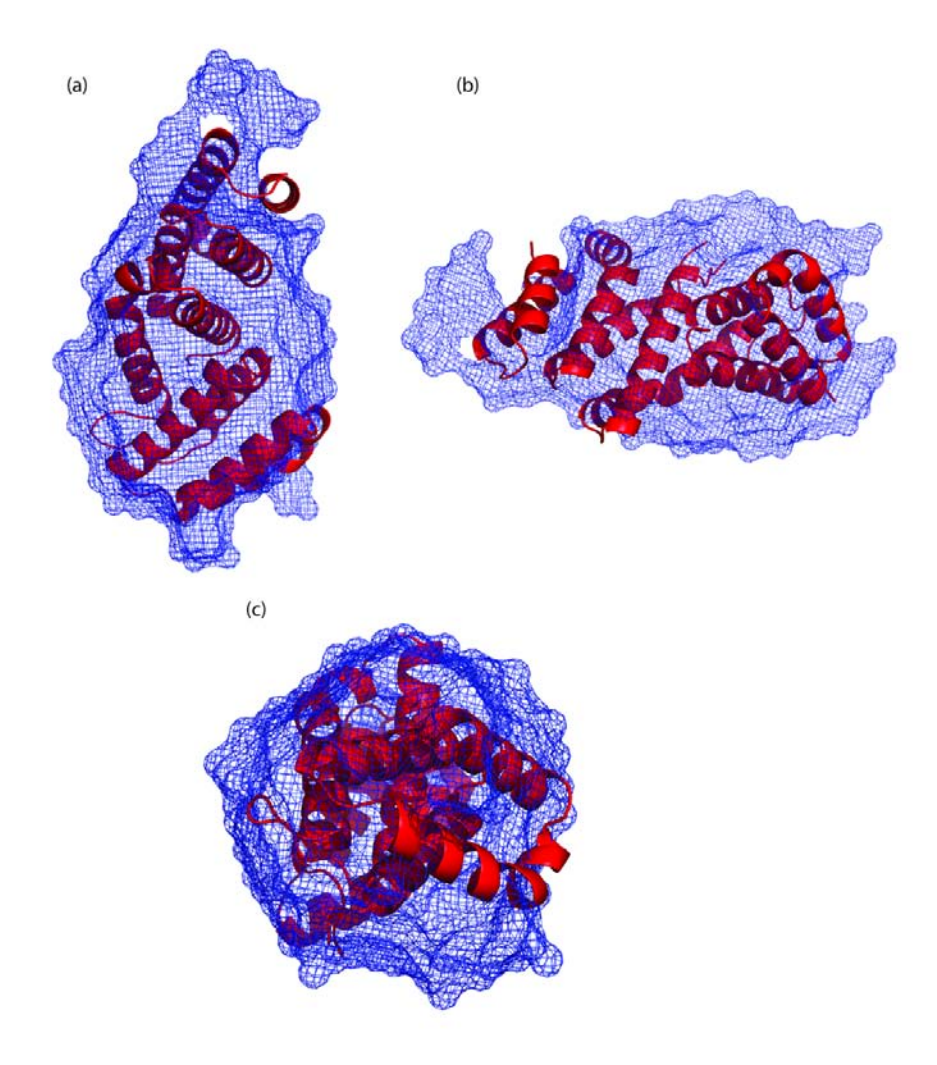


Figure 25 Three views of the MPaip1 SAXS model reconstructed *ab initio* using GASBOR (Svergun et al., 2001).

#### 4. CONCLUSION

In this study, the crystal structure of MPaip1 (Paip1 residues spanning 157-375) was determined at a resolution of 1.7 Å, revealing a crescent shaped deca-helical molecule that belongs to the HEAT-repeat family of proteins. MPaip1 consists of ten antiparallel α-helices of varying lengths which produce a molecule of dimensions: 59 Å (length) x 32 Å (depth) x 38 Å (width) (Figure 16). Heat-repeats are found in a number of proteins generally involved in a diverse array of cellular processes that are dependent on the association of sizable multi-protein complexes. MPaip1 has been implicated in the involvement of two putative multi-protein complexes. The better studied of these complexes is the translation initiation complex; where Paip1 acts as a translational enhancer by conferring a stabilizing effect on the mutli-factor complex which involves PABP, eIF4G, eIF4A and eIF4E among others. Paip1s interactions with PABP, eIF4A and eIF3 (Craig et al., 1998; Martineau et al., 2008) are thought to potentiate the circularization of mRNA which synergistically enhances translation (Gallie, 1991). The binding of Paip1 to eIF4A was originally described by Craig et al., however, here I show that the interaction is very weak relative to MIF4G (Craig et al., 1998). The weak interaction is attributed to the absence of the critical tryptophan residue which is absent from Paip1. This might suggest that the contact of Paip1 and eIF4A merely acts a stabilizing interaction in the multi-protein translation initiation complex. Moreover, unlike MIF4G, MPaip1 does not bind to eIF4A. This fact, coupled with differences in a number of helices between MIF4G and MPaip1 suggests that residues external to the MPaip1 domain may be critical to the stabilizing interaction with eIF4A in the translation initiation complex.

The second and lesser studied mutli-factor complex is the mCRD destabilizing complex (Chen et al., 1992). The mCRD is the major determinant of instability of mRNA which directs accelerated deadenylation and causes mRNA degradation (Grosset et al.,

2000). The mCRD has been shown to associate with the five proteins Paip1, PABP, Unr, hnRNP D and NSAP1 (Grosset et al., 2000). Overexpression of these proteins stabilizes mCRD-containing mRNA by impeding deadenylation (Grosset et al., 2000). As a result, the mCRD bridging complex is thought to be associated to the poly(A) tail via PABP, thus blocking the poly(A) tail from nuclease attack and preventing deadenylation. Outlining the conservation of residues among all known Paip1 species on the surface of MPaip1 revealed a number of scattered yet matching sequences which form a highly conserved contiguous patch on the surface (Figure 18). This conserved surface patch involves helices 2b,3b and 4b, which are stacked on top of each other via hydrophobic interactions (Figure 18). The surface patch is highly conserved, contiguous, and does not overlap with the eIF4A binding regions en masse. This may signify functional significance of as yet unknown functions of Paip1. The fact that residues external to the MPaip1 sequence are quite unstructured and flexible renders this region a possibility in mCRD complex association. Additionally, apart from elF4A and elF3, MIF4G has been shown to interact with both RNA (Pestova et al., 1996) and DNA (Kim et al., 1999). As a result, studies that target the binding of Paip1 to DNA and RNA may prove promising. Finally, successful surface reconstruction of MPaip1 using Small Angle X-ray Scattering shows that it is possible to study Paip1 in complex with any of its aforementioned associates.

٠.

### **REFERENCES**

- Adam, S.A., Nakagawa, T., Swanson, M.S., Woodruff, T.K., and Dreyfuss, G. (1986). mRNA polyadenylate-binding protein: gene isolation and sequencing and identification of a ribonucleoprotein consensus sequence. Mol Cell Biol *6*, 2932-2943.
- Andrade, M.A., and Bork, P. (1995). HEAT repeats in the Huntington's disease protein. Nat Genet *11*, 115-116.
- Andrade, M.A., Petosa, C., O'Donoghue, S.I., Muller, C.W., and Bork, P. (2001). Comparison of ARM and HEAT protein repeats. J Mol Biol *309*, 1-18.
- Aravind, L., and Koonin, E.V. (2000). Eukaryote-specific domains in translation initiation factors: implications for translation regulation and evolution of the translation system. Genome Res *10*, 1172-1184.
- Barton, G.J. (1990). Protein multiple sequence alignment and flexible pattern matching. Methods Enzymol *183*, 403-428.
- Beers, D.R., Henkel, J.S., Xiao, Q., Zhao, W., Wang, J., Yen, A.A., Siklos, L., McKercher, S.R., and Appel, S.H. (2006). Wild-type microglia extend survival in PU.1 knockout mice with familial amyotrophic lateral sclerosis. Proc Natl Acad Sci U S A *103*, 16021-16026.
- Berlanga, J.J., Baass, A., and Sonenberg, N. (2006). Regulation of poly(A) binding protein function in translation: Characterization of the Paip2 homolog, Paip2B. RNA *12*, 1556-1568.
- Birnboim, H.C., and Doly, J. (1979). A rapid alkaline extraction procedure for screening recombinant plasmid DNA. Nucleic Acids Res *7*, 1513-1523.
- Blaszczyk, L., Dutkiewicz, M., and Ciesiolka, J. (2007). [Translation of eukaryotic mRNA in a cap-independent mode]. Postepy Biochem *53*, 400-412.
- Brunger, A.T., Adams, P.D., Clore, G.M., DeLano, W.L., Gros, P., Grosse-Kunstleve, R.W., Jiang, J.S., Kuszewski, J., Nilges, M., Pannu, N.S., et al. (1998). Crystallography & NMR system: A new software suite for macromolecular structure determination. Acta Crystallogr D Biol Crystallogr 54, 905-921.

- Callaghan, M.J., Russell, A.J., Woollatt, E., Sutherland, G.R., Sutherland, R.L., and Watts, C.K. (1998). Identification of a human HECT family protein with homology to the Drosophila tumor suppressor gene hyperplastic discs. Oncogene *17*, 3479-3491.
- Chen, C.Y., You, Y., and Shyu, A.B. (1992). Two cellular proteins bind specifically to a purine-rich sequence necessary for the destabilization function of a c-fos protein-coding region determinant of mRNA instability. Mol Cell Biol *12*, 5748-5757.
- Cingolani, G., Petosa, C., Weis, K., and Muller, C.W. (1999). Structure of importin-beta bound to the IBB domain of importin-alpha. Nature *399*, 221-229.
- Clery, A., Blatter, M., and Allain, F.H. (2008). RNA recognition motifs: boring? Not quite. Curr Opin Struct Biol *18*, 290-298.
- Craig, A.W., Haghighat, A., Yu, A.T., and Sonenberg, N. (1998). Interaction of polyadenylate-binding protein with the eIF4G homologue PAIP enhances translation. Nature *392*, 520-523.
- Deo, R.C., Sonenberg, N., and Burley, S.K. (2001). X-ray structure of the human hyperplastic discs protein: an ortholog of the C-terminal domain of poly(A)-binding protein. Proc Natl Acad Sci U S A *98*, 4414-4419.
- Deprez, C., Lloubes, R., Gavioli, M., Marion, D., Guerlesquin, F., and Blanchard, L. (2005). Solution structure of the E.coli TolA C-terminal domain reveals conformational changes upon binding to the phage g3p N-terminal domain. J Mol Biol *346*, 1047-1057.
- Derry, M.C., Yanagiya, A., Martineau, Y., and Sonenberg, N. (2006). Regulation of poly(A)-binding protein through PABP-interacting proteins. Cold Spring Harb Symp Quant Biol *71*, 537-543.
- Doublie, S. (1997). Preparation of selenomethionyl proteins for phase determination. Methods Enzymol *276*, 523-530.
- Duncan, R., Milburn, S.C., and Hershey, J.W. (1987). Regulated phosphorylation and low abundance of HeLa cell initiation factor eIF-4F suggest a role in translational control. Heat shock effects on eIF-4F. J Biol Chem *262*, 380-388.

- Emsley, P., and Cowtan, K. (2004). Coot: model-building tools for molecular graphics. Acta Crystallogr D Biol Crystallogr *60*, 2126-2132.
- Fukada, Y., Yasui, K., Kitayama, M., Doi, K., Nakano, T., Watanabe, Y., and Nakashima, K. (2007). Gene expression analysis of the murine model of amyotrophic lateral sclerosis: studies of the Leu126delTT mutation in SOD1. Brain Res *1160*, 1-10.
- Gallie, D.R. (1991). The cap and poly(A) tail function synergistically to regulate mRNA translational efficiency. Genes Dev *5*, 2108-2116.
- Gingras, A.C., Gygi, S.P., Raught, B., Polakiewicz, R.D., Abraham, R.T., Hoekstra, M.F., Aebersold, R., and Sonenberg, N. (1999a). Regulation of 4E-BP1 phosphorylation: a novel two-step mechanism. Genes Dev 13, 1422-1437.
- Gingras, A.C., Raught, B., and Sonenberg, N. (1999b). eIF4 initiation factors: effectors of mRNA recruitment to ribosomes and regulators of translation. Annu Rev Biochem *68*, 913-963.
- Glickman, M.H., and Ciechanover, A. (2002). The ubiquitin-proteasome proteolytic pathway: destruction for the sake of construction. Physiol Rev 82, 373-428.
- Gorlach, M., Burd, C.G., and Dreyfuss, G. (1994). The mRNA poly(A)-binding protein: localization, abundance, and RNA-binding specificity. Exp Cell Res *211*, 400-407.
- Gradi, A., Imataka, H., Svitkin, Y.V., Rom, E., Raught, B., Morino, S., and Sonenberg, N. (1998). A novel functional human eukaryotic translation initiation factor 4G. Mol Cell Biol *18*, 334-342.
- Gray, N.K., Coller, J.M., Dickson, K.S., and Wickens, M. (2000). Multiple portions of poly(A)-binding protein stimulate translation in vivo. EMBO J *19*, 4723-4733.
- Grosset, C., Chen, C.Y., Xu, N., Sonenberg, N., Jacquemin-Sablon, H., and Shyu, A.B. (2000). A mechanism for translationally coupled mRNA turnover: interaction between the poly(A) tail and a c-fos RNA coding determinant via a protein complex. Cell *103*, 29-40.
- Groves, M.R., and Barford, D. (1999). Topological characteristics of helical repeat proteins. Curr Opin Struct Biol *9*, 383-389.

- Haghighat, A., and Sonenberg, N. (1997). eIF4G dramatically enhances the binding of eIF4E to the mRNA 5'-cap structure. J Biol Chem *272*, 21677-21680.
- Hannig, E.M. (1995). Protein synthesis in eukaryotic organisms: new insights into the function of translation initiation factor eIF-3. Bioessays *17*, 915-919.
- Hendrickson, W.A. (1991). Determination of macromolecular structures from anomalous diffraction of synchrotron radiation. Science *254*, 51-58.
- Hershko, A., and Ciechanover, A. (1998). The ubiquitin system. Annu Rev Biochem *67*, 425-479.
- Hinnebusch, A.G. (2006). eIF3: a versatile scaffold for translation initiation complexes. Trends Biochem Sci *31*, 553-562.
- Hochstrasser, M. (1996). Protein degradation or regulation: Ub the judge. Cell 84, 813-815.
- Holcik, M., and Sonenberg, N. (2005). Translational control in stress and apoptosis. Nat Rev Mol Cell Biol *6*, 318-327.
- Hosoda, N., Kobayashi, T., Uchida, N., Funakoshi, Y., Kikuchi, Y., Hoshino, S., and Katada, T. (2003). Translation termination factor eRF3 mediates mRNA decay through the regulation of deadenylation. J Biol Chem *278*, 38287-38291.
- Huibregtse, J.M., Scheffner, M., Beaudenon, S., and Howley, P.M. (1995). A family of proteins structurally and functionally related to the E6-AP ubiquitin-protein ligase. Proc Natl Acad Sci U S A *92*, 5249.
- Imataka, H., Gradi, A., and Sonenberg, N. (1998). A newly identified N-terminal amino acid sequence of human eIF4G binds poly(A)-binding protein and functions in poly(A)-dependent translation. EMBO J *17*, 7480-7489.
- Imataka, H., Olsen, H.S., and Sonenberg, N. (1997). A new translational regulator with homology to eukaryotic translation initiation factor 4G. EMBO J *16*, 817-825.
- Imataka, H., and Sonenberg, N. (1997). Human eukaryotic translation initiation factor 4G (eIF4G) possesses two separate and independent binding sites for eIF4A. Mol Cell Biol 17, 6940-6947.

- Ince, P.G., Tomkins, J., Slade, J.Y., Thatcher, N.M., and Shaw, P.J. (1998). Amyotrophic lateral sclerosis associated with genetic abnormalities in the gene encoding Cu/Zn superoxide dismutase: molecular pathology of five new cases, and comparison with previous reports and 73 sporadic cases of ALS. J Neuropathol Exp Neurol *57*, 895-904.
- Jacobson, A., and Favreau, M. (1983). Possible involvement of poly(A) in protein synthesis. Nucleic Acids Res *11*, 6353-6368.
- Jacobson, A., and Peltz, S.W. (1996). Interrelationships of the pathways of mRNA decay and translation in eukaryotic cells. Annu Rev Biochem *65*, 693-739.
- Johannes, G., Carter, M.S., Eisen, M.B., Brown, P.O., and Sarnow, P. (1999). Identification of eukaryotic mRNAs that are translated at reduced cap binding complex eIF4F concentrations using a cDNA microarray. Proc Natl Acad Sci U S A *96*, 13118-13123.
- Kadlec, J., Izaurralde, E., and Cusack, S. (2004). The structural basis for the interaction between nonsense-mediated mRNA decay factors UPF2 and UPF3. Nat Struct Mol Biol 11, 330-337.
- Kahvejian, A., Roy, G., and Sonenberg, N. (2001). The mRNA closed-loop model: the function of PABP and PABP-interacting proteins in mRNA translation. Cold Spring Harb Symp Quant Biol *66*, 293-300.
- Kahvejian, A., Svitkin, Y.V., Sukarieh, R., M'Boutchou, M.N., and Sonenberg, N. (2005). Mammalian poly(A)-binding protein is a eukaryotic translation initiation factor, which acts via multiple mechanisms. Genes Dev *19*, 104-113.
- Khaleghpour, K., Kahvejian, A., De Crescenzo, G., Roy, G., Svitkin, Y.V., Imataka, H., O'Connor-McCourt, M., and Sonenberg, N. (2001a). Dual interactions of the translational repressor Paip2 with poly(A) binding protein. Mol Cell Biol *21*, 5200-5213.
- Khaleghpour, K., Svitkin, Y.V., Craig, A.W., DeMaria, C.T., Deo, R.C., Burley, S.K., and Sonenberg, N. (2001b). Translational repression by a novel partner of human poly(A) binding protein, Paip2. Mol Cell *7*, 205-216.

- Kim, C.Y., Takahashi, K., Nguyen, T.B., Roberts, J.K., and Webster, C. (1999). Identification of a nucleic acid binding domain in eukaryotic initiation factor elFiso4G from wheat. J Biol Chem *274*, 10603-10608.
- Kim, K.M., Cho, H., Choi, K., Kim, J., Kim, B.W., Ko, Y.G., Jang, S.K., and Kim, Y.K. (2009). A new MIF4G domain-containing protein CTIF directs nuclear cap-binding protein CBP80/20-dependent translation. Genes Dev.
- Kobe, B., and Kajava, A.V. (2000). When protein folding is simplified to protein coiling: the continuum of solenoid protein structures. Trends Biochem Sci *25*, 509-515.
- Konarev, P.V., Volkov, V.V., Sokolova, A.V., Koch, M.H.J., and Svergun, D.I. (2003). PRIMUS: a Windows PC-based system for small-angle scattering data analysis. Journal of Applied Crystallography *36*, 1277-1282.
- Korneeva, N.L., Lamphear, B.J., Hennigan, F.L., Merrick, W.C., and Rhoads, R.E. (2001). Characterization of the two eIF4A-binding sites on human eIF4G-1. J Biol Chem *276*, 2872-2879.
- Kozlov, G., De Crescenzo, G., Lim, N.S., Siddiqui, N., Fantus, D., Kahvejian, A., Trempe, J.F., Elias, D., Ekiel, I., Sonenberg, N., et al. (2004). Structural basis of ligand recognition by PABC, a highly specific peptide-binding domain found in poly(A)-binding protein and a HECT ubiquitin ligase. EMBO J 23, 272-281.
- Kozlov, G., Trempe, J.F., Khaleghpour, K., Kahvejian, A., Ekiel, I., and Gehring, K. (2001). Structure and function of the C-terminal PABC domain of human poly(A)-binding protein. Proc Natl Acad Sci U S A *98*, 4409-4413.
- Kuersten, S., and Goodwin, E.B. (2003). The power of the 3' UTR: translational control and development. Nat Rev Genet *4*, 626-637.
- Lamphear, B.J., Kirchweger, R., Skern, T., and Rhoads, R.E. (1995). Mapping of functional domains in eukaryotic protein synthesis initiation factor 4G (eIF4G) with picornaviral proteases. Implications for cap-dependent and cap-independent translational initiation. J Biol Chem *270*, 21975-21983.

- LeFebvre, A.K., Korneeva, N.L., Trutschl, M., Cvek, U., Duzan, R.D., Bradley, C.A., Hershey, J.W., and Rhoads, R.E. (2006). Translation initiation factor elF4G-1 binds to elF3 through the elF3e subunit. J Biol Chem *281*, 22917-22932.
- Levy-Strumpf, N., Deiss, L.P., Berissi, H., and Kimchi, A. (1997). DAP-5, a novel homolog of eukaryotic translation initiation factor 4G isolated as a putative modulator of gamma interferon-induced programmed cell death. Mol Cell Biol *17*, 1615-1625.
- Linder, P., and Slonimski, P.P. (1989). An essential yeast protein, encoded by duplicated genes TIF1 and TIF2 and homologous to the mammalian translation initiation factor eIF-4A, can suppress a mitochondrial missense mutation. Proc Natl Acad Sci U S A 86, 2286-2290.
- Lorsch, J.R., and Herschlag, D. (1998). The DEAD box protein eIF4A. 1. A minimal kinetic and thermodynamic framework reveals coupled binding of RNA and nucleotide. Biochemistry 37, 2180-2193.
- Malik, H.S., Eickbush, T.H., and Goldfarb, D.S. (1997). Evolutionary specialization of the nuclear targeting apparatus. Proc Natl Acad Sci U S A *94*, 13738-13742.
- Marcotrigiano, J., Lomakin, I.B., Sonenberg, N., Pestova, T.V., Hellen, C.U., and Burley, S.K. (2001). A conserved HEAT domain within eIF4G directs assembly of the translation initiation machinery. Mol Cell *7*, 193-203.
- Martineau, Y., Derry, M.C., Wang, X., Yanagiya, A., Berlanga, J.J., Shyu, A.B., Imataka, H., Gehring, K., and Sonenberg, N. (2008). Poly(A)-binding protein-interacting protein 1 binds to eukaryotic translation initiation factor 3 to stimulate translation. Mol Cell Biol 28, 6658-6667.
- McCoy, A.J. (2007). Solving structures of protein complexes by molecular replacement with Phaser. Acta Crystallogr D Biol Crystallogr *63*, 32-41.
- McCoy, A.J., Grosse-Kunstleve, R.W., Adams, P.D., Winn, M.D., Storoni, L.C., and Read, R.J. (2007). Phaser crystallographic software. J Appl Crystallogr *40*, 658-674.
- Merrick, W.C. (2004). Cap-dependent and cap-independent translation in eukaryotic systems. Gene 332, 1-11.

- Morino, S., Imataka, H., Svitkin, Y.V., Pestova, T.V., and Sonenberg, N. (2000). Eukaryotic translation initiation factor 4E (eIF4E) binding site and the middle one-third of eIF4GI constitute the core domain for cap-dependent translation, and the C-terminal one-third functions as a modulatory region. Mol Cell Biol *20*, 468-477.
- Munroe, D., and Jacobson, A. (1990). mRNA poly(A) tail, a 3' enhancer of translational initiation. Mol Cell Biol *10*, 3441-3455.
- Muthukrishnan, S., Both, G.W., Furuichi, Y., and Shatkin, A.J. (1975). 5'-Terminal 7-methylguanosine in eukaryotic mRNA is required for translation. Nature *255*, 33-37.
- Nagai, K., Oubridge, C., Ito, N., Avis, J., and Evans, P. (1995). The RNP domain: a sequence-specific RNA-binding domain involved in processing and transport of RNA. Trends Biochem Sci *20*, 235-240.
- Ohlmann, T., Rau, M., Pain, V.M., and Morley, S.J. (1996). The C-terminal domain of eukaryotic protein synthesis initiation factor (eIF) 4G is sufficient to support cap-independent translation in the absence of eIF4E. EMBO J *15*, 1371-1382.
- Otwinowski, Z., and Minor, W. (1997). Processing of X-ray diffraction data collected in oscillation mode. Macromolecular Crystallography, Pt A *276*, 307-326.
- Oughtred, R., Bedard, N., Adegoke, O.A., Morales, C.R., Trasler, J., Rajapurohitam, V., and Wing, S.S. (2002). Characterization of rat100, a 300-kilodalton ubiquitin-protein ligase induced in germ cells of the rat testis and similar to the Drosophila hyperplastic discs gene. Endocrinology *143*, 3740-3747.
- Palatnik, C.M., Wilkins, C., and Jacobson, A. (1984). Translational control during early Dictyostelium development: possible involvement of poly(A) sequences. Cell *36*, 1017-1025.
- Pasinelli, P., and Brown, R.H. (2006). Molecular biology of amyotrophic lateral sclerosis: insights from genetics. Nat Rev Neurosci *7*, 710-723.
- Perez-Canadillas, J.M., Santoro, J., Campos-Olivas, R., Lacadena, J., Martinez del Pozo, A., Gavilanes, J.G., Rico, M., and Bruix, M. (2000). The highly refined solution structure

- of the cytotoxic ribonuclease alpha-sarcin reveals the structural requirements for substrate recognition and ribonucleolytic activity. J Mol Biol 299, 1061-1073.
- Pestova, T.V., and Hellen, C.U. (2000). The structure and function of initiation factors in eukaryotic protein synthesis. Cell Mol Life Sci *57*, 651-674.
- Pestova, T.V., Shatsky, I.N., and Hellen, C.U. (1996). Functional dissection of eukaryotic initiation factor 4F: the 4A subunit and the central domain of the 4G subunit are sufficient to mediate internal entry of 43S preinitiation complexes. Mol Cell Biol *16*, 6870-6878.
- Pickart, C.M., and Rose, I.A. (1985). Functional heterogeneity of ubiquitin carrier proteins. J Biol Chem *260*, 1573-1581.
- Ponting, C.P. (2000). Novel eIF4G domain homologues linking mRNA translation with nonsense-mediated mRNA decay. Trends Biochem Sci *25*, 423-426.
- Porath, J., Carlsson, J., Olsson, I., and Belfrage, G. (1975). Metal chelate affinity chromatography, a new approach to protein fractionation. Nature *258*, 598-599.
- Prevot, D., Darlix, J.L., and Ohlmann, T. (2003). Conducting the initiation of protein synthesis: the role of eIF4G. Biol Cell *95*, 141-156.
- Ray, B.K., Lawson, T.G., Kramer, J.C., Cladaras, M.H., Grifo, J.A., Abramson, R.D., Merrick, W.C., and Thach, R.E. (1985). ATP-dependent unwinding of messenger RNA structure by eukaryotic initiation factors. J Biol Chem *260*, 7651-7658.
- Reynolds, C., Damerell, D., and Jones, S. (2009). ProtorP: a protein-protein interaction analysis server. Bioinformatics *25*, 413-414.
- Rogers, G.W., Jr., Richter, N.J., Lima, W.F., and Merrick, W.C. (2001). Modulation of the helicase activity of eIF4A by eIF4B, eIF4H, and eIF4F. J Biol Chem *276*, 30914-30922.
- Rosen, D.R. (1993). Mutations in Cu/Zn superoxide dismutase gene are associated with familial amyotrophic lateral sclerosis. Nature *364*, 362.
- Rost, B., and Sander, C. (1993). Prediction of protein secondary structure at better than 70% accuracy. J Mol Biol 232, 584-599.

- Roy, G., De Crescenzo, G., Khaleghpour, K., Kahvejian, A., O'Connor-McCourt, M., and Sonenberg, N. (2002). Paip1 interacts with poly(A) binding protein through two independent binding motifs. Mol Cell Biol 22, 3769-3782.
- Rozen, F., Edery, I., Meerovitch, K., Dever, T.E., Merrick, W.C., and Sonenberg, N. (1990). Bidirectional RNA helicase activity of eucaryotic translation initiation factors 4A and 4F. Mol Cell Biol *10*, 1134-1144.
- Sachs, A.B., and Davis, R.W. (1989). The poly(A) binding protein is required for poly(A) shortening and 60S ribosomal subunit-dependent translation initiation. Cell *58*, 857-867.
- Sachs, A.B., Davis, R.W., and Kornberg, R.D. (1987). A single domain of yeast poly(A)-binding protein is necessary and sufficient for RNA binding and cell viability. Mol Cell Biol 7, 3268-3276.
- Schutz, P., Bumann, M., Oberholzer, A.E., Bieniossek, C., Trachsel, H., Altmann, M., and Baumann, U. (2008). Crystal structure of the yeast eIF4A-eIF4G complex: an RNA-helicase controlled by protein-protein interactions. Proc Natl Acad Sci U S A *105*, 9564-9569.
- Schwab, M. (1999). Oncogene amplification in solid tumors. Semin Cancer Biol 9, 319-325.
- Scotto, L., Narayan, G., Nandula, S.V., Subramaniyam, S., Kaufmann, A.M., Wright, J.D., Pothuri, B., Mansukhani, M., Schneider, A., Arias-Pulido, H., *et al.* (2008). Integrative genomics analysis of chromosome 5p gain in cervical cancer reveals target over-expressed genes, including Drosha. Mol Cancer *7*, 58.
- Shatkin, A.J. (1976). Capping of eucaryotic mRNAs. Cell 9, 645-653.
- Shyu, A.B., Greenberg, M.E., and Belasco, J.G. (1989). The c-fos transcript is targeted for rapid decay by two distinct mRNA degradation pathways. Genes Dev 3, 60-72.
- Sonenberg, N., and Hinnebusch, A.G. (2009). Regulation of translation initiation in eukaryotes: mechanisms and biological targets. Cell *136*, 731-745.
- Sorensen, C.M., and Shi, D. (2000). Guinier analysis for homogeneous dielectric spheres of arbitrary size. Optics Communications *178*, 31-36.

- Studier, F.W. (2005). Protein production by auto-induction in high density shaking cultures. Protein Expr Purif *41*, 207-234.
- Svergun, D.I. (1991). Mathematical-Methods in Small-Angle Scattering Data-Analysis. Journal of Applied Crystallography *24*, 485-492.
- Svergun, D.I. (1992). Determination of the Regularization Parameter in Indirect-Transform Methods Using Perceptual Criteria. Journal of Applied Crystallography *25*, 495-503.
- Svergun, D.I., Petoukhov, M.V., and Koch, M.H. (2001). Determination of domain structure of proteins from X-ray solution scattering. Biophys J *80*, 2946-2953.
- Svitkin, Y.V., and Sonenberg, N. (2006). [Translational control by the poly(A) binding protein: a check for mRNA integrity]. Mol Biol (Mosk) *40*, 684-693.
- Terwilliger, T.C. (2000). Maximum-likelihood density modification. Acta Crystallogr D Biol Crystallogr *56*, 965-972.
- Terwilliger, T.C., and Berendzen, J. (1999). Automated MAD and MIR structure solution. Acta Crystallogr D Biol Crystallogr *55*, 849-861.
- Vogelstein, B., and Gillespie, D. (1979). Preparative and analytical purification of DNA from agarose. Proc Natl Acad Sci U S A 76, 615-619.
- Waggoner, S.E. (2003). Cervical cancer. Lancet 361, 2217-2225.
- Wells, S.E., Hillner, P.E., Vale, R.D., and Sachs, A.B. (1998). Circularization of mRNA by eukaryotic translation initiation factors. Mol Cell 2, 135-140.
- Wickens, M. (1990). How the messenger got its tail: addition of poly(A) in the nucleus. Trends Biochem Sci *15*, 277-281.
- Wijesekera, L.C., and Leigh, P.N. (2009). Amyotrophic lateral sclerosis. Orphanet J Rare Dis 4, 3.
- Wisdom, R., and Lee, W. (1991). The protein-coding region of c-myc mRNA contains a sequence that specifies rapid mRNA turnover and induction by protein synthesis inhibitors. Genes Dev *5*, 232-243.
- Yamanaka, K., Boillee, S., Roberts, E.A., Garcia, M.L., McAlonis-Downes, M., Mikse, O.R., Cleveland, D.W., and Goldstein, L.S. (2008). Mutant SOD1 in cell types other than

motor neurons and oligodendrocytes accelerates onset of disease in ALS mice. Proc Natl Acad Sci U S A *105*, 7594-7599.

Yoshida, M., Yoshida, K., Kozlov, G., Lim, N.S., De Crescenzo, G., Pang, Z., Berlanga, J.J., Kahvejian, A., Gehring, K., Wing, S.S., *et al.* (2006). Poly(A) binding protein (PABP) homeostasis is mediated by the stability of its inhibitor, Paip2. EMBO J *25*, 1934-1944.